Journal of Geodynamics 114 (2018) 19–40

Contents lists available at ScienceDirect

Journal of Geodynamics

journal homepage: www.elsevier.com/locate/jog

Integrated elemental and Sr-Nd-Pb-Hf isotopic studies of Mesozoic mafic dykes from the eastern North China Craton: implications for the dramatic transformation of lithospheric mantle

Shen Liu[a,*], Caixia Feng[a], M. Santosh[a,b,c], Guangying Feng[d], Ian M. Coulson[e], Mengjing Xu[a], Zhuang Guo[a], Xiaolei Guo[a], Hao Peng[a], Qiang Feng[a]

[a] State Key Laboratory of Continental Dynamics Department of Geology, Northwest University, Xi'an 710069, PR China
[b] China University of Geosciences Beijing, Beijing 100083, PR China
[c] Department of Earth Sciences, University of Adelaide, Adelaide SA 5005, Australia
[d] Institute of Geology, Chinese Academy of Geological Sciences, Beijing 100037, PR China
[e] Solid Earth Studies Laboratory, Department of Geology, University of Regina, Regina, Saskatchewan S4S 0A2, Canada

ARTICLE INFO

Keywords:
Mafic dyke swarms
Geochemical and isotopic composition
Lithospheric evolution
Craton destruction
North China Craton

ABSTRACT

Evolution of the lithospheric mantle beneath the North China Craton (NCC) from its Precambrian cratonic architecture until Paleozoic, and the transformation to an oceanic realm during Mesozoic, with implications on the destruction of cratonic root have attracted global attention. Here we present geochemical and isotopic data on a suite of newly identified Mesozoic mafic dyke swarms from the Longwangmiao, Weijiazhuang, Mengjiazhuang, Jiayou, Huangmi, and Xiahonghe areas (Qianhuai Block) along the eastern NCC with an attempt to gain further insights on the lithospheric evolution of the region. The Longwangmiao dykes are alkaline with LILE (Ba and K)- and LREE-enrichment ($(La/Yb)_{N>}$ 4.3) and EM1-like Sr-Nd-Pb-Hf isotopic signature ($(^{87}Sr/^{86}Sr)_{i>}$ 0.706; $\varepsilon_{Nd}(t) < -6.3$, $(^{206}Pb/^{204}Pb)_{i} > 16.6$, $(^{207}Pb/^{204}Pb)_{i>}$ 15.4, $(^{208}Pb/^{204}Pb)_{i>}$ 36.8, $\varepsilon_{Hf}(t) < -22.4$). The Weijiazhuang dykes are sub-alkaline with LILE (Ba and K)- and LREE-enrichment ($(La/Yb)_{N} > 3.7$), and display similar EM1-like isotopic features ($(^{87}Sr/^{86}Sr)_{i>}$ 0.706; $\varepsilon_{Nd}(t) < -7.0$, $(^{206}Pb/^{204}Pb)_{i} > 16.7$, $(^{207}Pb/^{204}Pb)_{i>}$ 15.4, $(^{208}Pb/^{204}Pb)_{i>}$ 36.9, $\varepsilon_{Hf}(t) < -23.3$). The Mengjiazhuang dykes are also sub-alkaline with LILE (Ba and K)- and LREE-enrichment ($(La/Yb)_{N} > 2.4$) and EM1-like isotopic features($(^{87}Sr/^{86}Sr)_{i>}$ 0.706; $\varepsilon_{Nd}(t) < -18.4$, $(^{206}Pb/^{204}Pb)_{i} > 16.7$, $(^{207}Pb/^{204}Pb)_{i>}$ 15.4, $(^{208}Pb/^{204}Pb)_{i>}$ 36.9, $\varepsilon_{Hf}(t) < -8.6$). The Jiayou dykes also display sub-alkaline affinity with LILE (Ba and K)- and LREE-enrichment ($(La/Yb)_{N} > 3.7$) and EM1-like Sr-Nd-Pb-Hf isotopic features ($(^{87}Sr/^{86}Sr)_{i>}$ 0.706; $\varepsilon_{Nd}(t) < -15.3$, $(^{206}Pb/^{204}Pb)_{i} > 16.7$, $(^{207}Pb/^{204}Pb)_{i>}$ 15.4, $(^{208}Pb/^{204}Pb)_{i>}$ 36.9, $\varepsilon_{Hf}(t) < -18.4$). The Huangmi dykes are alkaline (with $Na_2O + K_2O$ ranging to more than 5.9 wt.%)) with LILE (Ba and K)- and LREE-enrichment ($(La/Yb)_{N} > 9.3$) and EM1-like isotopic composition ($(^{87}Sr/^{86}Sr)_{i>}$ 0.705; $\varepsilon_{Nd}(t) < -15.1$, $(^{206}Pb/^{204}Pb)_{i} > 16.9$, $(^{207}Pb/^{204}Pb)_{i>}$ 15.5, $(^{208}Pb/^{204}Pb)_{i>}$ 36.9, $\varepsilon_{Hf}(t) < -12.2$). The Xiahonghe dykes are alkaline with LILE (Ba and K)- and LREE-enrichment ($(La/Yb)_{N} = 2.12\text{-}2.84$) and similar EM1-like Sr-Nd-Pb-Hf isotopic signature ($(^{87}Sr/^{86}Sr)_{i} > 0.705$; $\varepsilon_{Nd}(t) < -18.0$, $(^{206}Pb/^{204}Pb)_{i} > 16.9$, $(^{207}Pb/^{204}Pb)_{i>}$ 15.5, $(^{208}Pb/^{204}Pb)_{i>}$ 36.9, $\varepsilon_{Hf}(t) < -8.6$). Our data from the various mafic dyke suites suggest that the magmas were derived from EM1-like lithospheric mantle, corresponding to lithospheric mantle modified by the previously foundered lower crust beneath the eastern NCC. Our results suggest contrasting lithospheric evolution from Triassic (212 Ma) to Cretaceous (123 Ma) beneath the NCC. These mafic dykes mark an important phase of lithospheric thinning in the eastern North China Craton.

1. Introduction

Following its cratonization during Neoarchean through the assembly of several micro-blocks (Yang and Santosh, 2017), the North China Craton (NCC) remained as a relatively stable craton until Mesozoic when there was extensive reactivation, magmatism and craton destruction (Menzies et al., 2007; Griffin et al., 1998; Xu, 2001; Liu et al., 2005; Zheng et al., 2006; Gao et al., 2002, 2004, 2008, 2009; Wu et al., 2003a,b, 2005, 2006a,b; Zhang,

* Corresponding author.
E-mail address: liushen@vip.gyig.ac.cn (S. Liu).

https://doi.org/10.1016/j.jog.2017.11.007
Received 4 June 2017; Received in revised form 10 November 2017; Accepted 12 November 2017
Available online 28 November 2017

2005; Yang et al., 2008). This was also accompanied by the formation of wide-spread extensional basins (Zhu et al., 2008), detachment fault zones and metamorphic core complexes (Liu et al., 2008a,b,c, 2009), large-scale mineralization (Nie et al., 2010; Zhai, 2010; Li and Santosh, 2017), generation of adakites and bimodal volcanic rocks (Xiong et al., 2011), and large-scale mafic dykes (Liu, 2004; Liu et al., 2008a,b,c, 2009, 2010, 2013; Wu et al., 2008; Zhai et al., 2004; Dong et al., 2007). Thus, the evolution of the lithospheric mantle of the NCC has been a topic of wide interest, particularly following the documentation of a dramatic change from Paleozoic cratonic mantle to Cenozoic "oceanic" lithospheric mantle (Griffin et al., 1992, 1998; Xu, 2001; O'Reilly et al., 2001; Zhang et al., 2003a,b). This transformation warrants sizeable lithospheric thinning, which is considered to have occurred in the Mesozoic (Menzies and Xu, 1998; Lu et al., 2000, 2006; Gao et al., 2002; Zhang et al., 2003a,b; Wu et al., 2000, 2008; Zhang et al., 2007; Zheng et al., 2007). However, the mechanism leading to this change remains controversial, and various models proposed include the destabilization of the cratonic lithosphere through India-Eurasia collision (Menzies et al., 1993), and replacement of the Archean cratonic lithosphere by young Phanerozoic lithosphere resulting in removal of the Archean lithospheric keel (Zheng, 1999; Zheng et al., 2001; Poudjom Djomani et al., 2001). Some studies suggest that the lithospheric replacement might have occurred as early as Paleoproterozoic (1.9 Ga), based on Re-Os isotopic data on mantle xenoliths entrained in basalts (Gao et al., 2002). Several studies have proposed thermo-mechanical erosion from the base of the lithosphere and subsequent chemical erosion resulting from asthenosphere upwelling (Menzies and Xu, 1998; Xu, 2001; Xu et al., 2004; Wu et al., 2008; Santosh, 2010). The subduction of oceanic crust beneath both the northern and southern margins of the NCC in the Paleozoic (Meng and Zhang, 2000; Davis et al., 2001; Ren et al., 20002) is considered to be responsible for destabilization of the eastern NCC and the resulting thinning and replacement of the lithospheric mantle (Zhang et al., 2003a,b). The delamination of thickened lithosphere is also considered as an important mechanism leading to the Mesozoic lithospheric thinning (Gao et al., 1992, 1998a,b, 2002, 2004; Wu et al., 2003a,b, 2005, 2006a,b; Xu et al., 2006, 2008; Liu et al., 2008a,b,c, 2009). Investigations on Mesozoic extensional structures in the NCC have also provided important information on the lithospheric thinning (Wang et al., 2007a,b; Wu et al., 2008). In spite of the various mechanisms proposed including peridotite-melt interaction (Zhang et al., 2002, 2007; Tang et al., 2008; Zhang, 2009), magma extraction (Chen et al., 2004) and hydration (Niu, 2005), the replacement process remains enigmatic.

Mesozoic magmatism is widespread in the NCC, and the distribution of these magmatic suites shows both temporal and spatial regularity. The middle-early Triassic magmatic suites are mainly distributed in the northern margin of the NCC (Yinshan-Yanshan-western Liaoning, Yanji-northern Liaoning) whereas those between middle-late Triassic and early Jurassic are mainly located along the Yinshan-Yanshi-western Liaoning, Yanji-northern Liaoning, Liaodong Peninsula, Korean Peninsula, the western Hills of Beijing, little Qinling Mountains and western Shandong. The Middle-late Jurassic magmatic rocks are mainly distributed in the Yanshan-western Liaoning, Liaodong Peninsula, Jiaodong Peninsula and western Hilis of Beijing, and those of early Cretaceous occur along the eastern NCC, with the western boundary reaching up to the western margin of the Ordos Basin. The rock types include extrusive volcanics (basalt), shallow volcanic suites (rhyolite porphyry, andesite porphyry and trachyte porphyry), and hypabyssal rocks (granite, granite porphyry and syenite porphyry, and plutonic rocks (granodiorite, syenite porphyry, diorite, mafic dyke, and syenite). Furthermore, more than 300 mafic dykes were identified in the Liaoning Province, the Inner Mongolia Autonomous Region, Shanxi Province, Hebei Province, Shandong Province, Henan Province, Gansu and Shaanxi Province (Regional Geology of Hebei Province, Beijing, Tianjin, 1982; Regional Geology of Liaoning Province, 1989; Regional Geology of Shanxi Province, 1989; Regional Geology of Henan Province, 1989; Rgional Geology of Gansu Province, 1989; Regional Geology of Shaanxi Province, 1989; Regional Geology of Inner Mongolia Autonomous Region, 1991; Yang et al., 2007a,b; Liu et al., 2010). More than 150 mafic dykes (110-220 Ma) occur in the Hebei province including those around the Weichang, Chicheng, Fengning, Yixian, Laiyuan, Luxian, Quyang, Lingshou, Fuping, Yanliao, Fanshan, Zhuolu, and Sanchakou areas (Yang, 1991; Mu and Yan, 1992; Mu et al., 2001; Shao and Zhang, 2002; Shao et al., 2005; Liu et al., 2010; Yang et al., 2012, 2013; Yang, 2013; Tang, 2013; Tang et al., 2014). These Triassic-Cretaceous dykes provide an excellent opportunity to probe the underlying lithospheric mantle. In this study, we selected a suite of newly-discovered mafic dykes from this region within the Xingtai County (Fig. 1b) for detailed elemental-isotopic analysis. Our new data provide important constraints on the origin of the Mesozoic dykes and on their mantle sources beneath the eastern NCC. Using these data, together with those from previously published works from this region, we attempt to identify the spatio-temporal variations in the Mesozoic lithospheric mantle across the eastern NCC.

2. Regional geology

The NCC is one of the major Archean cratonic nuclei in Asia and preserves vestiges of crustal records ranging up to 3.8 Ga age (Liu et al., 1992; Zheng et al., 2005; Zhai and Santosh, 2011). The Archean tectonic architecture of the NCC is considered to be a mosaic of several microcontinental blocks (Zhai and Bian, 2000; Zhao, 2009), and recent studies have confirmed extensive magmatism and high grade metamorphism associated with the subduction-collision tectonics and suturing of the microblocks (Yang et al., 2016; Yang and Santosh, 2017). The NCC has been traditionally divided into the Eastern Block and the Western Block, which amalgamated along the Paleoproterozoic Trans-North China Orogen (Zhao et al., 2001, 2002, 2005; Wilde et al., 2002; Guo et al., 2005; Yang and Santosh, 2015). The Precambrian crystalline basement in the NCC is dominantly composed of tonalite-trondhjemite-granodiorite (TTG) gneisses together with metavolcanic and metasedimentary rocks, covered by Sinian-Ordovician marine sedimentary rocks, Carboniferous-Permian continental clastic rocks, and Mesozoic basin deposits (Zhao et al., 2002; Zhang et al., 2003a,b). The Western Block is composed of the Yinshan Block in the north and the Ordos Block to the south, separated by the E-W-trending Paleoproterozoic Inner Mongolia Suture Zone, also known as the Khondalite Belt (Xia et al., 2008; Yin et al., 2009, 2011; Li et al., 2011; Wang et al., 2011; Santosh et al., 2012). The Eastern Block consists of the Longgang (also known as the Yanliao Block) and Langrim blocks, separated by the Paleoproterozoic Jiao-Liao-Ji Belt (Li et al., 2006; Li and Zhao, 2007; Zhou et al., 2008; Zhao et al., 2010, 2012; Tam et al., 2012a,b; Zhao and Zhai, 2013).

In the Western Block, the cratonic lithosphere has been relatively stable sine Precambrian. In contrast, extensive magmatic activity occurred in the Eastern Block after its cratonization (Zhang et al., 2003a,b). The NCC is bound on the south by the Palaeozoic to Triassic Qinling-Dabie-Sulu Orogenic Belt (Li et al., 1993; Meng and Zhang, 2000; Zhang et al., 2003a,b; Dong and Santosh, 2016) and on the north by the Central Asian Orogenic Belt (Davis et al., 2001). The Qinling-Dabie-Sulu Orogenic Belt resulted from the continental collision between the NCC and the Yangtze Craton in the Triassic (Li et al., 1993). The EW-trending Central Asian Orogenic Belt was formed through south-directed subduction and arc-arc, arc-continent, and continent-continent collision mainly during the Palaeozoic (Robinson et al., 1999; Davis et al., 2001; Zhang et al., 2003a,b). During this time, multiple Ordovician to Permian oceanic arcs and the Mongolian microcontinent were amalgamated to the active margin of the NCC (Davis et al., 2001; Zhang et al., 2003a,b; Safonova et al.,2017).

In the present study, we analyzed Mesozoic mafic dykes from the Longwangmian, Weijiazhuang, Mengjiazhuang, Jiayou, Huangmi, and Xiahonghe in the Qianhuai Block of the eastern NCC (Fig. 1a). These dykes belong to three major periods of magmatic activity (212.0-199.6 Ma, 136.4 Ma, 123.5 Ma; Table 1; Fig. 2-2).

3. Petrography

Mafic dykes are widespread in the areas investigated in this study such as the Longwangmian, Weijiazhuang, Mengjiazhuang, Jiayou,

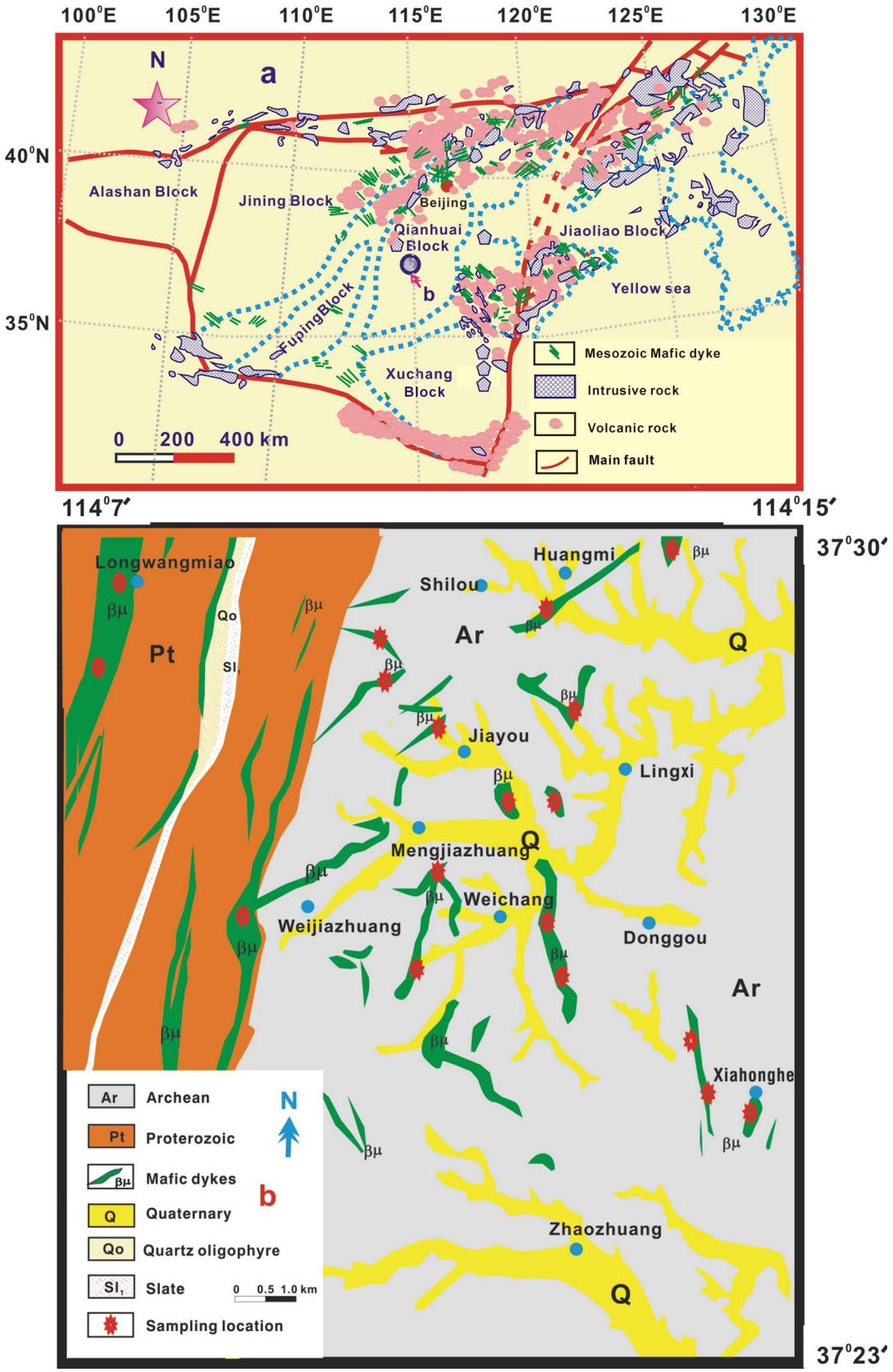

Fig. 1. (a) Simplified geological map showing the major tectonic units of the North China Craton and its surrounding areas (Santosh, 2010). (b) Schematic illustration showing the distribution of Mesozoic mafic dykes along the eastern NCC and sampling locations.

Huangmi, and Xiahonghe in the eastern NCC (Fig. 1b). The major rock types in these areas are granite, monzonite, and gneissic country rocks, all of which are intruded by mafic dykes, although the majority of the dykes are hosted by Archean-Proterozoic units (Fig. 1b). Individual mafic dykes studied are vertical, strike NE-SW, N-S, and E-W (Fig. 1b), and are between 0.1 km and 0.8 km in width, with lengths of 0.3-

Table 1
Zircon LA-ICP-MS U-Pb isotopic data for samples in the study areas from the eastern NCC.

LWM01						Isotopic	ratios					Age (Ma)					
Spot	Th	U	Pb	Th/U	$^{238}U/^{232}Th$	$^{207}Pb/^{206}Pb$	1s	$^{207}Pb/^{235}U$	1s	$^{206}Pb/^{238}U$	1s	$^{207}Pb/^{206}Pb$	1s	$^{207}Pb/^{235}U$	1s	$^{206}Pb/^{238}U$	1s
1	457	451	408	1.01	0.46	0.0517	0.0015	0.2283	0.0064	0.0335	0.0004	270	42	209	5	212	2
2	4085	2698	187	1.51	1.51	0.0517	0.0017	0.2278	0.0067	0.0335	0.0005	273	41	208	6	212	3
3	547	565	14.9	0.97	0.63	0.0506	0.0015	0.2256	0.0033	0.0336	0.0004	223	15	207	3	213	2
4	124	49.5	16.5	2.50	2.5	0.0519	0.0016	0.2264	0.0064	0.0331	0.0005	281	38	207	5	210	3
5	276	147	29.4	1.88	1.88	0.0518	0.0013	0.2274	0.0055	0.0333	0.0003	276	39	208	5	211	2
6	170	156	26.6	1.09	1.09	0.0516	0.0014	0.2281	0.0060	0.0334	0.0004	269	39	209	5	212	2
7	69.3	55.2	29.9	1.26	0.46	0.0517	0.0016	0.2283	0.0066	0.0334	0.0005	270	39	209	5	212	3
8	163	148	24.1	1.10	0.47	0.0518	0.0016	0.2272	0.0063	0.0333	0.0005	274	38	208	5	211	3
9	200	179	28.6	1.12	0.53	0.0507	0.0015	0.2258	0.0035	0.0335	0.0005	225	16	207	3	212	3
10	133	127	22.1	1.05	0.37	0.0515	0.0016	0.2288	0.0064	0.0336	0.0005	261	38	209	5	213	3
11	303	85.5	63.3	3.55	3.55	0.0515	0.0016	0.2294	0.0064	0.0335	0.0005	261	38	210	5	212	3
12	61.3	63.1	8.63	0.97	0.84	0.0508	0.0016	0.2236	0.0033	0.0336	0.0004	232	16	205	3	213	2
–																	
WJZ02						**Isotopic**	**ratios**					**Age (Ma)**					
Spot	Th	U	Pb	Th/U	$^{238}U/^{232}Th$	$^{207}Pb/^{206}Pb$	1s	$^{207}Pb/^{235}U$	1s	$^{206}Pb/^{238}U$	1s	$^{207}Pb/^{206}Pb$	1s	$^{207}Pb/^{235}U$	1s	$^{206}Pb/^{238}U$	1s
1	457	451	396	1.01	1.38	0.0521	0.0018	0.2268	0.0044	0.0316	0.0004	288	22	208	4	200	3
2	68.5	23.9	14.2	2.87	5.13	0.0501	0.0017	0.2174	0.0041	0.0315	0.0004	201	21	200	3	200	3
3	198	12.6	19.3	15.65	1.98	0.0544	0.0019	0.2372	0.0052	0.0316	0.0005	388	25	216	4	201	3
4	375	73.2	62.7	5.13	2.29	0.0505	0.0021	0.2194	0.0066	0.0315	0.0005	219	42	201	5	200	3
5	429	204	55.1	2.11	2.18	0.0527	0.0018	0.2281	0.0046	0.0314	0.0004	315	23	209	4	199	3
6	3587	1399	210	2.56	2.66	0.0506	0.0016	0.2182	0.0035	0.0313	0.0004	220	17	200	3	199	3
7	66.8	23.4	13.6	2.86	1.36	0.0519	0.0016	0.2265	0.0036	0.0316	0.0004	281	16	207	3	201	3
8	811	640	245	1.27	1.01	0.0499	0.0017	0.2149	0.0066	0.0312	0.0004	191	80	198	6	198	3
9	222	120	15.3	1.86	1.33	0.0523	0.0017	0.2248	0.0042	0.0312	0.0004	297	21	206	4	198	3
10	457	451	396	1.01	1.85	0.0519	0.0020	0.2244	0.0058	0.0314	0.0005	281	34	206	5	199	3
11	190.7	11.8	18.4	16.10	2.36	0.0523	0.0020	0.2282	0.0058	0.0317	0.0005	297	32	209	5	201	3
12	747	403	53.3	1.85	2.03	0.0506	0.0019	0.2200	0.0054	0.0315	0.0005	223	31	202	4	200	3
13	84.7	30.3	17.0	2.79	1.28	0.0511	0.0019	0.2215	0.0057	0.0314	0.0005	244	33	203	5	199	3
–																	
MJZ02						**Isotopic**	**ratios**					**Age (Ma)**					
Spot	Th	U	Pb	Th/U	$^{238}U/^{232}Th$	$^{207}Pb/^{206}Pb$	1s	$^{207}Pb/^{235}U$	1s	$^{206}Pb/^{238}U$	1s	$^{207}Pb/^{206}Pb$	1s	$^{207}Pb/^{235}U$	1s	$^{206}Pb/^{238}U$	1s
1	8136	1701	217	4.78	5.72	0.0494	0.0016	0.1447	0.0024	0.0212	0.0003	169	17	137	2	135	2
2	1980	681	68.6	2.91	2.2	0.0499	0.0017	0.1473	0.0031	0.0214	0.0003	192	24	140	3	136	2
3	93.7	73.5	5.52	1.28	4.89	0.0483	0.0013	0.1421	0.0034	0.0213	0.0003	113	66	135	3	136	2
4	3876	678	102	5.72	1.37	0.0525	0.0017	0.1586	0.0026	0.0219	0.0003	306	17	150	2	140	2
5	1471	668	46.2	2.20	2.23	0.0493	0.0022	0.1415	0.0058	0.0208	0.0003	160	101	134	5	133	2
6	3630	742	99.8	4.89	1.22	0.0493	0.0027	0.1458	0.0066	0.0215	0.0004	162	75	138	6	137	2
7	2893	2120	81.1	1.37	1.89	0.0514	0.0028	0.1528	0.0079	0.0216	0.0003	257	126	144	7	138	2
8	1265	568	33.6	2.23	3.65	0.0487	0.0016	0.1427	0.0025	0.0212	0.0003	135	19	135	2	135	2
9	290	73.9	22.1	3.92	1.01	0.0500	0.0018	0.1491	0.0037	0.0216	0.0003	195	31	141	3	138	2
10	274	225	10.2	1.22	3.88	0.0491	0.0022	0.1446	0.0052	0.0213	0.0003	155	55	137	5	136	2
11	374	198	11.9	1.89	0.31	0.0488	0.0018	0.1449	0.0034	0.0216	0.0003	136	29	137	3	137	2
12	2510	688	57.7	3.65	0.38	0.0518	0.0018	0.1520	0.0033	0.0213	0.0003	275	25	144	3	136	2
–																	
JY01						**Isotopic**	**ratios**					**Age (Ma)**					
Spot	Th	U	Pb	Th/U	$^{238}U/^{232}Th$	$^{207}Pb/^{206}Pb$	1s	$^{207}Pb/^{235}U$	1s	$^{206}Pb/^{238}U$	1s	$^{207}Pb/^{206}Pb$	1s	$^{207}Pb/^{235}U$	1s	$^{206}Pb/^{238}U$	1s
1	806	137	292	5.88	2.76	0.0498	0.0016	0.1475	0.0032	0.0215	0.0003	192	25	140	3	137	2
2	2573	2090	302	1.23	2.75	0.0482	0.0014	0.1423	0.0035	0.0214	0.0003	114	32	135	3	136	2
3	952	27.7	422	34.36	2.77	0.0524	0.0018	0.1585	0.0027	0.0218	0.0004	306	19	149	2	139	3
4	474	36.5	240	12.99	2.77	0.0494	0.0021	0.1416	0.0057	0.0207	0.0003	160	66	134	5	132	2
5	164	58.0	9.8	2.82	2.77	0.0492	0.0026	0.1457	0.0065	0.0216	0.0004	162	73	138	6	137	2
6	457	451	396	1.01	2.76	0.0515	0.0027	0.1527	0.0079	0.0217	0.0003	257	90	144	7	138	2
7	454	86.7	224	5.23	2.77	0.0486	0.0017	0.1428	0.0026	0.0213	0.0003	135	20	136	2	136	2
8	587	38.7	217	15.15	2.77	0.0502	0.0018	0.1492	0.0038	0.0217	0.0004	195	28	141	3	139	3
9	415	293	179	1.42	2.75	0.0494	0.0023	0.1447	0.0053	0.0214	0.0003	155	56	137	5	136	2
10	686	248	199	2.77	2.76	0.0486	0.0017	0.1448	0.0035	0.0215	0.0003	136	31	137	3	137	2
–																	
HM03						**Isotopic**	**ratios**					**Age (Ma)**					
Spot	Th	U	Pb	Th/U	$^{238}U/^{232}Th$	$^{207}Pb/^{206}Pb$	1s	$^{207}Pb/^{235}U$	1s	$^{206}Pb/^{238}U$	1s	$^{207}Pb/^{206}Pb$	1s	$^{207}Pb/^{235}U$	1s	$^{206}Pb/^{238}U$	1s
1	1459	352	52.9	4.14	4.14	0.0524	0.0028	0.1226	0.0057	0.0194	0.0003	303	78	117	5	124	2
2	628	188	24.5	3.34	3.34	0.0516	0.0027	0.1232	0.0059	0.0187	0.0004	268	71	118	5	119	3
3	865	321	32.0	2.69	2.12	0.0519	0.0025	0.1253	0.0058	0.0196	0.0003	281	78	120	5	125	2
4	569	160	26.1	3.55	2.12	0.0461	0.0027	0.1254	0.0071	0.0193	0.0003		97	120	6	123	2
5	714	346	49.8	2.07	2.12	0.0518	0.0029	0.1236	0.0056	0.0196	0.0003	277	73	118	5	125	2
6	99.3	48.2	5.1	2.06	2.12	0.0525	0.0028	0.1248	0.0056	0.0189	0.0003	307	73	119	5	121	2
7	449	445	387	1.01	2.12	0.0524	0.0027	0.1235	0.0055	0.0191	0.0003	303	73	118	5	122	2
8	2608	751	73.3	3.47	2.13	0.0526	0.0028	0.1235	0.0055	0.0198	0.0003	312	74	118	5	126	2
9	534	218	17.7	2.45	2.12	0.0523	0.0026	0.1229	0.0062	0.0192	0.0003	299	87	118	6	123	2
10	1543	364	64.1	4.24	2.13	0.0522	0.0024	0.1232	0.0061	0.0191	0.0003	294	84	118	6	122	2
11	1263	441	113	2.86	2.12	0.0521	0.0024	0.1226	0.0061	0.0196	0.0003	290	86	117	6	125	2
12	640	241	46.2	2.66	2.12	0.0523	0.0025	0.1221	0.0056	0.0195	0.0003	299	76	117	5	124	2
–																	
XHH01						**Isotopic**	**ratios**					**Age (Ma)**					
Spot	Th	U	Pb	Th/U	$^{238}U/^{232}Th$	$^{207}Pb/^{206}Pb$	1s	$^{207}Pb/^{235}U$	1s	$^{206}Pb/^{238}U$	1s	$^{207}Pb/^{206}Pb$	1s	$^{207}Pb/^{235}U$	1s	$^{206}Pb/^{238}U$	1s

(*continued on next page*)

Table 1 (*continued*)

LWM01						Isotopic	ratios					Age (Ma)					
1	457	450	398	1.01	1.58	0.0554	0.0028	0.1225	0.0056	0.0195	0.0003	428	74	117	5	124	2
2	208	106	90.6	1.96	1.57	0.0517	0.0027	0.1233	0.0058	0.0186	0.0004	272	69	118	5	119	3
3	71.3	61.2	12.6	1.16	1.58	0.0518	0.0025	0.1254	0.0058	0.0195	0.0003	277	78	120	5	124	2
4	358	227	26.6	1.58	1.58	0.0462	0.0027	0.1253	0.0072	0.0194	0.0003	5	99	120	6	124	2
5	413	351	20.9	1.18	1.58	0.0519	0.0029	0.1235	0.0057	0.0195	0.0004	281	66	118	5	124	3
6	583	403	54.0	1.45	1.58	0.0526	0.0028	0.1247	0.0055	0.0188	0.0003	312	71	119	5	120	2
7	178	107	10.8	1.67	1.58	0.0525	0.0027	0.1236	0.0056	0.0192	0.0003	307	75	118	5	123	2
8	263	53.4	18.8	4.93	1.57	0.0525	0.0028	0.1234	0.0054	0.0197	0.0003	307	72	118	5	126	2
9	522	132	157	3.95	1.58	0.0524	0.0026	0.1289	0.0063	0.0193	0.0004	303	74	123	6	123	3
10	171	140	8.87	1.22	1.56	0.0521	0.0024	0.1233	0.0062	0.0192	0.0003	290	86	118	6	123	2
11	236	123	16.9	1.92	1.56	0.0522	0.0024	0.1225	0.0061	0.0195	0.0003	294	86	117	6	124	2

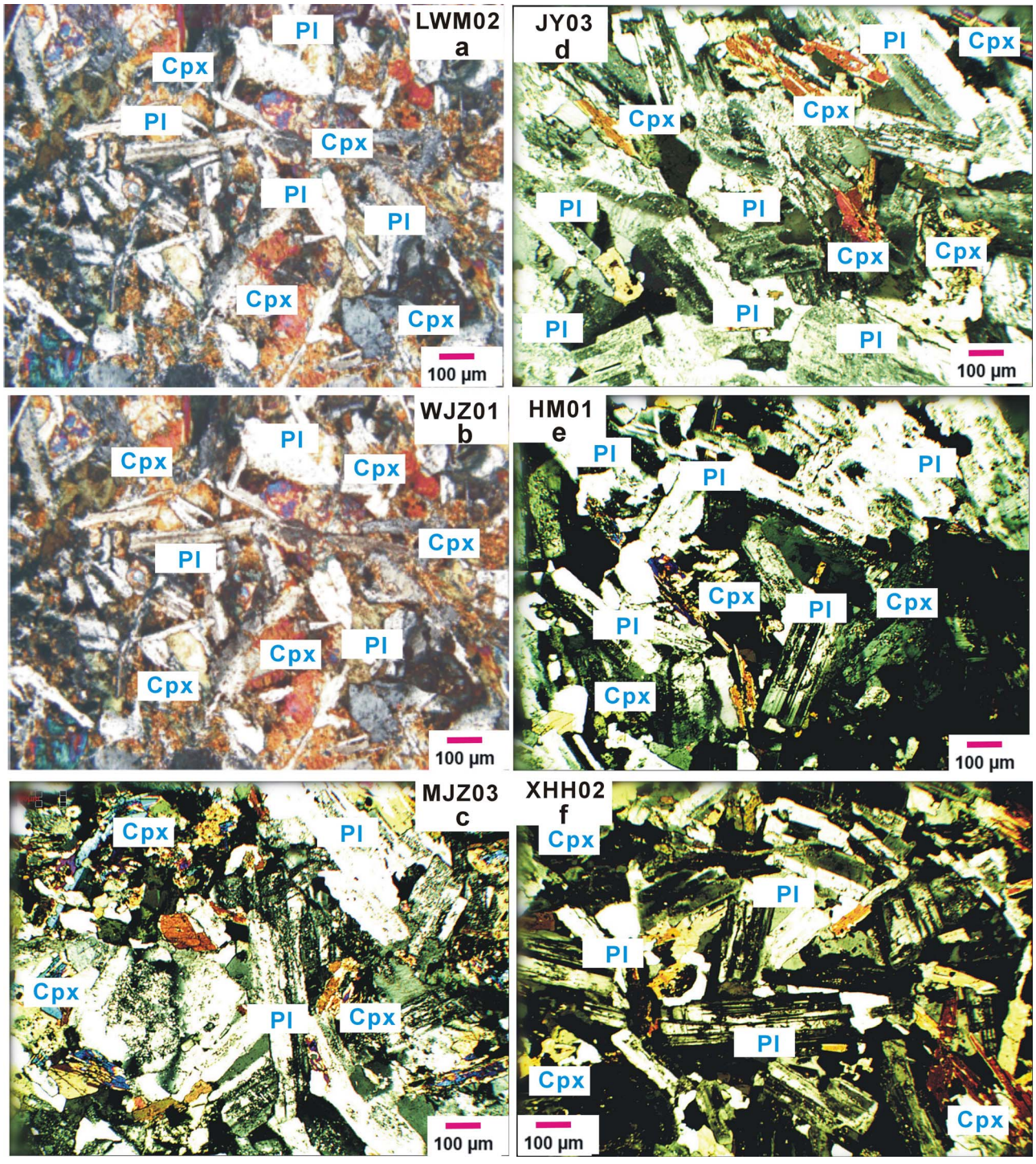

Fig. 2.

6.0 km (Fig. 1b). The rocks are dark grey, show typical massive and diabasic structure. Under thin section, the major mineral constituents are slender, columnar and euhedral plagioclase (50 vol %), and clinopyroxene (45 vol %) with accessory opaques, minor interstitial quartz between the plagioclase grains and secondary chlorite (Fig. 2).

The mafic dykes in Longwangmiao were emplaced into Proterozoic units, are vertical, with NW-SE strike, and show widths of 0.2-0.8 km and lengths of 1.5-6.0 km (Fig. 1b). They contain 30%-36% of combined clinopyroxene and, plagioclase (together constituting 30-35 vol %), with, and minor biotiteic microphenocrysts (0.5-1.2 mm) within a groundmass (~65%-70%) of pyroxene, plagioclase, magnetite, and chlorite (Fig. 2a).

The mafic dykes studied within the Weijiazhuang and Mengjiazhuang areas are mostly emplaced into Archean units, and are sub-alkalic, vertical, strikinge N-S, and NE-SW, and are 0.1-0.6 km wide and 0.3-1.2 km long (Fig. 1b). They contain 30%-35% of show clinopyroxene, alkali feldspar, and plagioclase, and with minor biotitic microphenocrysts (0.5-1.3 mm) (total 30-35 vol %), within a groundmass (~60%-65%) of pyroxene, alkali feldspar, plagioclase, and magnetite (Fig. 2b, c).

Mafic dykes studied from the Jiayou and Huangmi areas were emplaced into Archean units, are sub-alkalic and alkalic, vertical, strikinge E-W, and NE-SW, and have widths of 0.1-0.3 km and lengths of 0.5-1.5 km (Fig. 1b). They are characterized by clinopyroxene, alkali feldspar, plagioclase, and minor biotite microphenocrysts (0.5-1.2 mm) (total 30-35 vol %), in a groundmass (~60%) of pyroxene, alkali feldspar, plagioclase, and magnetite (Fig. 2d, e).

Mafic dykes from Xiahonghe were also emplaced into Archean units, are alkalic, vertical, striking N-S and NW-SE, and are 0.1-0.6 km wide and 0.6-2.0 km long (Fig. 1b). They contain microphenocrysts (0.5-1.0 mm) of clinopyroxene, plagioclase, and minor biotite (total 30-35 vol %) within a groundmass (~65%-70%) of pyroxene, plagioclase, magnetite, and chlorite (Fig. 2f).

The Longwangmiao (Triassic, 212.0 ± 1.4 Ma (zircon U-Pb age), 215.3 Ma (whole-rock K-Ar age)), Huangmi and Xiahonghe (late Cretaceous, 123.5 ± 1.2 Ma (zircon U-Pb age), 125.3 Ma (whole-rock K-Ar age), 123.3 ± 1.3 Ma (zircon U-Pb age), 125.6 Ma (whole-rock K-Ar age)) dykes are alkalic, whereas the others are sub-alkalic. The presence of alkali pyroxene, zeolite, feldspar and olivine rather than orthopyroxene, augite, and quartz in the mafic dykes from Longwangmiao, Huangmi and Xiahonghe confirm this inference.

4. Analytical methods

Zircon grains were extracted using a combined technique of heavy liquid and magnetic separation, and then handpicked under a binocular microscope, mounted in epoxy resin and polished until the grain centers were exposed. To reveal their internal structures, cathodoluminescence (CL) imaging was undertaken using a Quanta 400FEG environmental scanning electron microscope equipped with an Oxford energy dispersive spectroscopy system and a Gatan CL3+ detector (Fig. 3-1). The zircon U-Pb dating was conducted on an Agilent 7500a ICP-MS instrument equipped with a 193 nm ArF-excimer laser and a homogenizing, imaging optical system. Zircon 91500 was used as a standard and NIST 610 was used to optimize the results. Fixed spot size of 30 μm with a laser repetition rate of 6 Hz was adopted throughout this study. Analytical methodology is described in detail in Yuan et al. (2004). Common-Pb corrections were made using the method of Andersen (2002). Data were processed using the GLITTER 4.0 and ISOPLOT (Ludwig, 2003) programs. Errors on individual analyses by LA-ICP-MS are quoted at the 95% (1σ) confidence level. Fresh samples were powdered, and the whole-rock K-Ar age were analyzed at the K-Ar age laboratory of the Institute of Geology, China Seismological Bureau. An MM-1200 mas spectrograph was used for the K-Ar age determination, and the extraction system was set-up by the VG corp. The constants are adopted as $\lambda = 5.543*10^{-10}/a$, $\lambda_e = 0.58*10^{-10}/a$, $\lambda_\beta = 0.58*10^{-10}/a$, $^{40}K/^{38}K = 1.167\text{-}10^{-4}/mol/g$ (Table 2). In situ zircon Hf isotopic analyses were performed on a Nu Plasma HR MC-ICP-MS equipped with a GeoLas 2005 193 nm ArF-excimer laser-ablation system. Analyses were carried out using spot size of 44 μm and He was also used as carrier gas. The laser repetition rate is 10 Hz and the energy density applied is 15–20 J/cm^{-2}. During the analysis, the $^{176}Hf/^{177}Hf$ ratio of the standard zircon (91500) were 0.282295 ± 0.000027 (n = 14, 2σ), which is in good agreement with the recommended $^{176}Hf/^{177}Hf$ ratio within 2σ (0.2823075 ± 58, 2σ; 0.282015 ± 0.000029, 2σ) (Griffin et al., 2006; Wu et al., 2006a,b). All the above analysis were performed at the Key state Laboratory of Continental Dynamics, Northwest University, Xi'an, China. Major

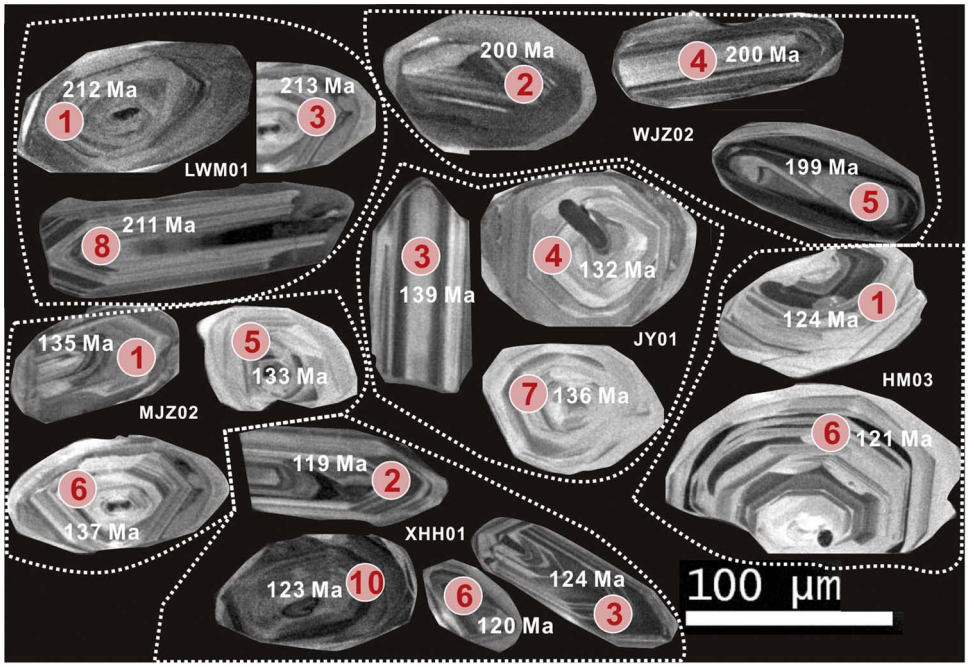

Fig. 3. Zircon cathodoluminescence images (2-1) and LA-ICP-MS U-Pb concordia diagrams (2-2) for the mafic dykes in the present study areas from the eastern NCC.

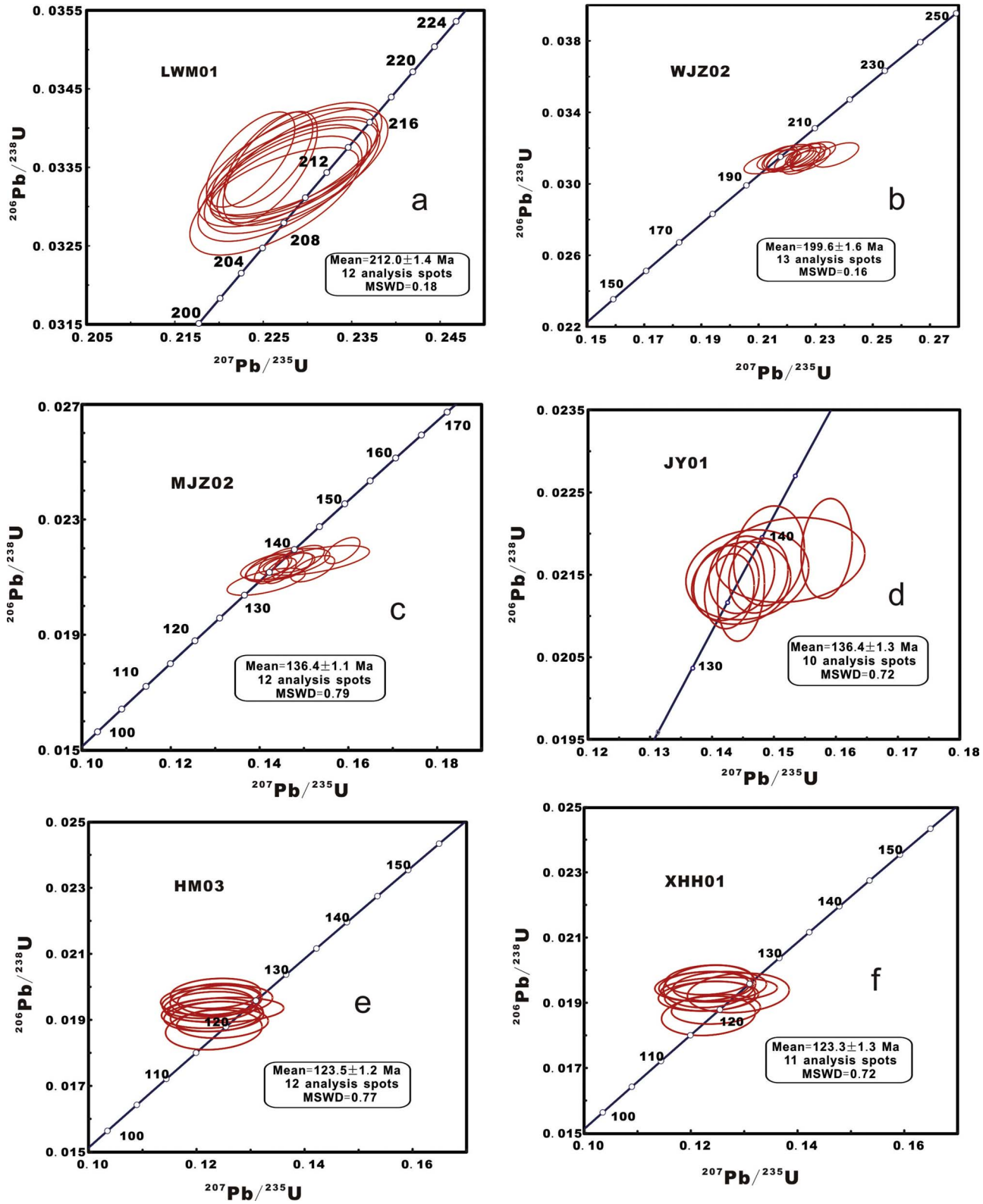

Fig. 3. (*continued*)

oxides were analyzed with a PANalytical Axios-advance X-ray fluorescence spectrometer (XRF) at the State Key Laboratory of Ore Deposit Geochemistry (LODG), Institute of Geochemistry, Chinese Academy of Science. Fused glass disks were used and the analytical precision as determined on the Chinese National standard GSR-3 was better than 5% (Table 3). Loss on ignition (LOI) was obtained using 1 g powder heated up to 1100 °C for 1 h. Trace elements were performed with a ELAN 6000 ICP-MS at the LODG, following procedures described by Qi et al. (2000). The discrepancy between triplicate analyses is less than 5% for all elements. Analyses of international standards OU-6 and GBPG-1 are in good agreement with recommended values (Table 4). For Rb-Sr and Sm-Nd isotope analyses, sample powders were spiked with mixed

Table 2
Whole-rock K-Ar ages of the mafic dykes.

Sample	Rock type	Dating method	K (%)	$^{40}Ar_{rad}$ *10^{-10}/mol*g^{-1}	$^{40}Ar_{rad}$ (%)	Age (Ma ± 1δ)
LWM03	dolerite	whole-rock (K-Ar)	0.43	1.43	92.45	215.3 ± 4.6
WJZ02	dolerite	whole-rock (K-Ar)	0.39	1.38	92.36	204.5 ± 5.2
MJZ04	dolerite	whole-rock (K-Ar)	1.95	4.75	92.33	138.2 ± 3.3
JY03	dolerite	whole-rock (K-Ar)	1.74	4.17	96.08	137.4 ± 2.8
HM01	dolerite	whole-rock (K-Ar)	1.65	3.72	95.13	125.3 ± 2.4
XHH02	dolerite	whole-rock (K-Ar)	1.14	2.52	90.34	125.6 ± 2.7

Table 3
Major element (wt.%) compositions of the mafic dykes in the study areas form the eastern NCC.

Sample	SiO_2	TiO_2	Al_2O_3	Fe_2O_3	MnO	MgO	CaO	K_2O	Na_2O	P_2O_5	LOI	Total	$Mg^{\#}$
LWM01	49.47	0.95	14.91	12.93	0.17	6.09	9.53	1.83	3.34	0.26	0.44	99.92	62
LWM02	49.29	0.97	14.79	13.06	0.17	6.32	9.04	1.87	3.38	0.26	0.37	99.52	60
LWM03	49.36	0.93	14.75	13.22	0.18	6.47	9.83	1.84	2.78	0.26	0.32	99.94	62
LWM04	48.68	1.15	14.68	13.07	0.19	6.53	9.08	1.84	3.41	0.27	0.97	99.87	60
LWM05	50.90	0.91	14.56	12.51	0.17	6.63	9.19	1.85	2.86	0.25	0.39	100.22	62
LWM06	49.46	0.89	14.46	13.13	0.17	6.86	10.40	1.76	2.79	0.22	0.25	100.39	64
LWM07	50.63	1.04	13.62	13.01	0.17	6.16	10.29	1.85	2.28	0.14	0.67	99.86	64
WJZ01	50.55	0.68	14.63	10.38	0.16	8.07	10.59	1.82	1.94	0.15	0.87	99.84	69
WJZ02	47.65	0.54	14.06	10.87	0.15	11.11	9.81	1.85	1.77	0.12	1.35	99.28	67
WJZ06	48.54	0.63	16.38	10.50	0.14	7.78	10.35	1.84	2.14	0.14	1.21	99.65	68
MJZ03	49.43	0.89	13.96	13.92	0.20	7.04	11.20	1.94	1.56	0.08	0.23	100.45	64
MJZ04	48.97	0.87	13.89	13.79	0.20	7.08	11.13	1.98	1.67	0.08	0.32	99.98	64
MJZ05	49.22	0.85	13.89	13.69	0.20	7.15	11.11	1.96	1.64	0.08	0.31	100.10	64
MJZ11	47.55	0.98	14.27	14.03	0.20	8.19	8.91	2.08	1.87	0.09	0.92	99.09	58
MJZ18	49.59	1.33	13.14	14.96	0.20	6.13	10.59	1.93	1.85	0.12	0.31	100.15	61
MJZ25	49.89	1.30	13.22	15.02	0.20	6.17	10.48	1.95	1.73	0.11	0.19	100.26	61
MJZ27	50.13	1.28	13.18	15.18	0.20	6.06	10.50	1.93	1.62	0.12	0.15	100.35	60
MJZ28	50.18	1.31	13.17	15.25	0.20	6.13	10.46	1.94	1.46	0.12	0.16	100.38	60
MJZ31	50.45	1.29	12.85	15.24	0.20	6.02	9.53	1.96	1.52	0.13	0.33	99.52	58
MJZ32	49.98	1.29	13.13	14.89	0.20	5.97	10.25	1.94	1.81	0.12	0.36	99.94	60
MJZ35	50.16	1.32	13.01	15.39	0.20	6.12	9.83	1.93	1.71	0.13	0.14	99.94	58
MJZ36	50.20	1.29	13.06	15.31	0.20	6.11	9.69	1.95	1.83	0.12	0.18	99.94	60
MJZ42	49.97	1.24	13.20	14.88	0.19	6.37	10.56	1.92	1.52	0.11	0.19	100.15	61
MJZ44	50.43	1.11	13.40	14.50	0.20	6.10	10.41	1.93	1.56	0.12	0.15	99.91	63
MJZ46	51.57	1.09	13.22	14.16	0.19	5.88	9.91	1.92	1.42	0.14	0.14	99.64	65
JY03	49.16	1.17	14.31	14.87	0.19	6.25	8.54	1.96	1.85	0.19	0.32	98.81	59
JY07	48.58	1.17	14.25	14.61	0.20	6.26	9.67	1.97	1.78	0.19	0.45	99.13	62
JY12	49.41	1.19	14.32	14.67	0.19	6.09	9.55	1.96	1.69	0.19	0.35	99.61	62
JY13	49.68	1.15	13.90	14.55	0.20	6.58	9.34	1.95	1.58	0.18	0.36	99.47	61
JY14	49.34	1.16	14.41	14.61	0.19	6.18	9.24	1.93	1.46	0.19	0.82	99.53	61
JY15	49.15	0.67	14.93	12.59	0.25	7.43	9.01	1.97	1.88	0.15	1.25	99.28	64
HM01	47.70	2.87	18.26	12.11	0.03	6.58	2.45	2.46	3.45	1.05	2.33	99.29	54
HM03	46.98	2.71	17.29	11.95	0.03	8.09	2.49	2.53	3.39	1.17	2.28	98.91	60
XHH02	48.87	1.31	12.92	15.40	0.19	6.67	9.46	1.98	2.46	0.13	0.26	99.65	60
XHH03	48.48	1.22	14.47	14.74	0.20	6.15	9.71	1.96	2.54	0.19	0.21	99.87	62
XHH04	49.34	1.24	12.83	13.89	0.19	5.68	10.67	1.94	2.46	0.12	0.82	99.18	66
XHH05	49.53	1.29	12.95	15.16	0.20	6.05	10.16	1.96	2.35	0.12	0.15	99.92	62

isotope tracers, dissolved in Teflon capsules with HF + HNO_3 acids, and separated by conventional cation-exchange technique (Zhang et al., 2001). Isotopic measurement was performed on the MAT-262 TIMS at the Institute of Geology and Geophysics (Table 5), Chinese Academy of Sciences. Procedural blanks were < 100 pg for Sm and Nd and < 500 pg for Rb and Sr. The mass fractionation correction for Sr and Nd isotopic ratios were based on $^{86}Sr/^{88}Sr = 0.1194$ and $^{146}Nd/^{144}Nd = 0.7219$, respectively. Analyses of standards during the period of analysis are as follows: NBS987 gave $^{86}Sr/^{88}Sr = 0.710245 \pm 14$ (2σ); La Jolla gave $^{143}Nd/^{144}Nd = 0.511861 \pm 19$ (2σ). Pb was separated and purified by conventional cation-exchange technique with diluted HBr as eluant. Detailed sample preparation and analytical procedure follow Zhang et al. (2002). The Pb isotopic ratios were measured with the MAT-262 TIMS at the IGG (Table 5), analyses of standard NBS981 during the period of analysis yielded $^{204}Pb/^{206}Pb = 0.0897 \pm 15$, $^{207}Pb/^{206}Pb = 0.91445 \pm 80$, and $^{208}Pb/^{206}Pb = 2.1617 \pm 200$.

5. Results

5.1. Zircon geochronology

Zircon is commonly present in the studied mafic dykes, and all the grains show oscillatory or planar zoning in CL images (Fig. 3-1), indicating a magmatic origin. None of the grains show evidence of inherited cores and all have relatively high Th/U ratios (0.97-34.4, 0.97-3.55 for the Longwangmiao dykes, 1.01-16.1 for the Weijiazhuang dykes, 1.22-5.72 for the Mengjiazhuang dykes, 1.01-34.4 for the Jiayou dykes, 1.01-4.14 for the Huangmi dykes, and 1.01-4.93 for the Xiahonghe dykes), which also indicate a magmatic origin. The zircon U-Pb age data indicate that the Longwangmiao dykes were emplacedat 212.0 ± 1.4 Ma (n = 12, MSWD = 0.18), the Weijiazhuang dykes at 199.6 ± 1.6 Ma (n = 13, MSWD = 0.16), the Mengjiazhuang dykes at 136.4 ± 1.1 Ma (n = 12, MSWD = 0.79), the Jiayou at 136.4 ± 1.3 Ma (n = 10, MSWD = 0.72), those from Huangmi at 123.5 ± 1.2 Ma (n = 12, MSWD = 0.77), and the dykes from Xiahonghe at

Table 4
Trace element (ppm) compositions of the mafic dykes in the study areas from the eastern NCC.

Sample	Sc	V	Cr	Ga	Ba	Rb	Sr	Y	Zr	Hf	Nb	Ta	Th	U	Pb	La	Ce	Pr	Nd	Sm	Eu	Gd	Tb	Dy	Ho	Er	Tm	Yb	Lu	$(La/Yb)_N$	Eu_N/Eu^*
LWM01	29.3	256	180	16.5	304	22.3	252	21.7	74	1.93	3.83	0.23	0.52	0.2	5.15	17.3	35.3	4.42	19.1	3.66	1.16	3.68	0.51	3.51	0.78	2.21	0.33	2.08	0.32	5.97	0.97
LWM02	31.6	249	180	15.4	456	33.5	242	19.8	71	1.81	3.62	0.24	0.52	0.16	3.21	15.3	32.3	4.18	17.5	3.79	1.11	3.82	0.56	3.49	0.77	2.14	0.33	2.09	0.31	5.25	0.89
LWM03	30.6	263	190	16.9	254	17.7	271	20.4	74	1.83	3.61	0.22	0.56	0.11	3.18	15.1	32.2	4.19	17.9	3.72	1.12	3.75	0.57	3.56	0.77	2.24	0.33	2.17	0.33	4.99	0.92
LWM04	30.4	252	180	15.7	200	15.2	240	19.9	71	1.94	3.53	0.21	0.53	0.11	4.22	14.2	30.5	4.15	17.1	3.91	1.09	3.74	0.55	3.51	0.76	2.18	0.34	2.15	0.33	4.74	0.87
LWM05	29.3	239	200	16	389	31.6	262	20.6	76	1.82	3.61	0.22	0.53	0.1	4.24	14.5	30.6	4.11	17.8	3.72	1.17	3.67	0.54	3.42	0.74	2.22	0.32	2.09	0.31	4.98	0.97
LWM06	32.3	264	200	15.6	105	6.02	242	18.4	60	1.52	3.63	0.23	0.47	0.09	4.17	11.6	24.6	3.42	14.6	3.23	1.04	3.29	0.49	3.12	0.67	1.99	0.31	1.91	0.32	4.38	0.98
LWM07	38.1	296	160	17.4	236	13.8	257	25.8	108	2.83	4.35	0.32	1.72	0.35	4.15	14.3	30.2	3.88	16.6	3.98	1.06	3.52	0.52	3.41	0.72	2.21	0.31	2.04	0.32	5.03	0.87
WJZ01	31.5	213	770	13.9	69.5	3.72	196	12.3	45	1.22	2.52	0.23	0.41	0.06	1.21	7.81	16.9	2.28	10.5	2.42	0.78	2.51	0.35	2.21	0.49	1.45	0.22	1.48	0.23	3.79	0.97
WJZ02	25.3	168	740	13.5	281	15.7	185	10.4	37	1.06	2.05	0.14	0.36	0.04	2.13	10.5	14.4	1.89	8.04	1.95	0.63	2.03	0.27	1.81	0.4	1.17	0.17	1.43	0.18	5.27	0.97
WJZ06	25.2	183	170	15.6	42.8	2.53	240	12.3	46	1.22	2.43	0.13	0.43	0.05	1.75	9.16	17.1	2.19	9.91	2.22	0.66	2.3	0.32	2.16	0.47	1.29	0.2	1.35	0.21	4.87	0.89
MJZ03	45.2	345	130	16.8	67.4	10.4	138	20.2	59	1.73	2.81	0.24	0.68	0.19	2.28	8.71	14.9	2.21	10.3	2.55	0.86	3.41	0.56	3.43	0.77	2.23	0.34	2.18	0.35	2.87	0.89
MJZ04	45.1	321	130	16.2	48.1	9.51	133	19.6	58	1.71	2.72	0.22	0.72	0.22	2.16	8.53	14.4	2.17	10.2	2.69	0.88	3.51	0.57	3.76	0.84	2.39	0.36	2.38	0.36	2.57	0.88
MJZ05	44.3	329	140	17.4	71.3	14.1	138	20.5	59	1.72	2.83	0.23	0.69	0.2	3.24	8.62	15.3	2.22	9.85	2.54	0.88	3.34	0.55	3.64	0.79	2.21	0.33	2.15	0.33	2.88	0.92
MJZ11	47.2	361	130	20.4	146	33.4	135	29.2	69	1.92	3.25	0.23	0.79	0.26	3.28	13.1	22.4	2.76	14.2	3.62	1.33	5.12	0.77	4.82	1.06	3.05	0.43	2.77	0.43	3.39	0.94
MJZ18	44.4	428	100	19.4	37.1	1.5	146	28.1	91	2.53	4.24	0.32	1.17	0.27	2.33	11.2	21.2	2.83	14.3	3.8	1.21	4.62	0.76	5.1	1.12	3.1	0.46	3.01	0.46	2.67	0.88
MJZ25	45.2	445	110	20.1	33.8	1.61	155	28.1	92	2.51	4.42	0.31	1.21	0.28	3.09	11.6	22.5	3.15	13.4	3.73	1.24	4.52	0.75	5.05	1.11	3.13	0.46	2.96	0.47	2.81	0.92
MJZ27	44.3	406	100	19	45.5	1.72	130	27	90	2.54	4.03	0.31	1.21	0.28	15.3	10.4	20.6	3.04	14.2	3.98	1.24	4.77	0.77	4.89	1.08	3.16	0.47	3.06	0.46	2.44	0.87
MJZ28	45.1	436	100	19.7	53.5	2.43	140	27.5	86	2.45	4.12	0.33	1.21	0.26	1.82	10.8	21.3	3.13	13.7	3.69	1.19	4.32	0.72	4.77	1.06	3.09	0.44	2.89	0.44	2.68	0.91
MJZ31	44.2	439	100	19.7	70.3	9.31	147	28.2	94	2.43	4.33	0.32	1.23	0.32	1.64	12.1	23.5	3.23	14.6	3.89	1.31	4.94	0.78	4.83	1.12	3.21	0.47	2.98	0.48	2.91	0.91
MJZ32	44.4	433	100	20.9	77.5	4.93	133	29.9	98	2.62	4.32	0.32	1.32	0.33	1.73	11.3	23.3	3.19	14.6	3.78	1.26	4.87	0.81	4.99	1.14	3.22	0.49	3.04	0.46	2.67	0.90
MJZ35	44.3	409	90.2	18.7	61.7	7.82	141	26.6	88	2.54	4.15	0.31	1.19	0.28	1.42	11.4	22.2	3.06	14.2	3.8	1.26	4.62	0.71	4.82	1.06	3.13	0.47	2.84	0.46	2.88	0.92
MJZ36	43.4	429	100	19.3	69.8	2.11	133	28.1	91	2.53	4.13	0.33	1.19	0.27	4.11	11.4	21.6	3.03	14.4	3.67	1.22	4.55	0.75	4.84	1.11	3.16	0.46	2.93	0.47	2.79	0.91
MJZ42	43.2	411	120	18.9	33.4	1.53	148	25.6	83	2.21	3.91	0.24	1.06	0.27	13.3	10.4	20.6	2.93	13.3	3.59	1.17	4.15	0.69	4.36	0.98	2.82	0.42	2.71	0.43	2.75	0.93
MJZ44	42.6	362	100	20.1	42.6	2.21	161	27.6	89	2.33	3.92	0.33	1.14	0.26	2.19	10.9	22.1	3.12	13.8	3.57	1.16	4.44	0.73	4.71	1.05	2.94	0.43	2.73	0.43	2.86	0.89
MJZ46	43.3	307	110	18.8	42.7	2.14	161	30.9	103	3.04	4.73	0.31	1.49	0.34	6.08	12.3	25.2	3.25	16.1	4.25	1.51	5.41	0.89	5.61	1.32	3.71	0.53	3.45	0.54	2.56	0.96
JY03	37.3	308	80.2	21	91.7	6.12	290	23.4	86	2.51	4.42	0.32	1.03	0.22	4.22	14.1	29.9	4.13	18	4.49	1.46	4.84	0.7	4.31	0.94	2.68	0.40	2.52	0.36	4.01	0.96
JY07	36.1	304	80.4	21.4	37.9	1.91	308	23.9	88	2.44	4.31	0.33	1.04	0.16	2.31	13.7	30.3	3.82	17.6	4.52	1.36	4.52	0.68	4.32	0.94	2.63	0.39	2.48	0.39	3.96	0.92
JY12	38.4	308	80.2	19.8	54.7	2.72	287	23.9	88	2.61	4.24	0.32	0.97	0.25	1.64	14.2	31.7	3.96	18	4.54	1.46	5.01	0.75	4.54	1.01	2.8	0.43	2.72	0.39	3.74	0.94
JY13	37.3	308	80.3	19.4	58.6	3.71	253	23.6	86	2.42	4.06	0.31	0.97	0.23	1.52	13.1	29.4	3.83	17.7	4.46	1.35	4.69	0.67	4.16	0.95	2.63	0.34	2.38	0.34	3.95	0.90
JY14	37.2	301	80.1	19.5	108	5.22	295	23.3	85	2.43	4.32	0.32	1.05	0.29	2.18	16.8	34.8	4.4	19.2	4.53	1.58	4.84	0.72	4.39	0.97	2.65	0.34	2.26	0.31	5.33	1.03
JY15	34.5	257	250	15.2	93.3	4.04	204	15.3	34	1.07	1.63	0.13	0.29	0.05	2.25	8.62	16.5	2.24	9.33	2.38	0.84	2.87	0.43	2.78	0.59	1.75	0.26	1.74	0.26	3.55	0.98
HM01	28.2	246	20.3	36.1	718	88.8	1857	93.5	520	13.5	20.4	1.71	17.9	5.61	3.23	104	226	27.4	117	27.3	7.09	24.9	3.37	19.6	3.79	9.47	1.28	7.48	1.14	9.97	0.83
HM03	30.3	248	20.5	36.8	743	93.5	1962	77.8	524	13.3	19.5	1.82	18.3	4.76	4.14	88.6	201	24.3	107	23.6	6.25	20.9	2.78	15.6	3.15	7.89	1.09	6.78	1.04	9.37	0.86
XHH02	43.1	428	120	18.8	349	22.4	135	28.1	87	2.52	4.14	0.32	1.21	0.25	2.15	9.14	19.7	2.63	11.7	3.51	1.07	4.56	0.73	4.63	1.06	3.02	0.45	2.91	0.45	2.25	0.82
XHH03	36.5	312	80.2	21.1	69.9	4.32	305	23.8	91	2.34	4.31	0.33	1.04	0.35	3.06	9.39	22.3	3.03	14.2	3.86	1.42	4.65	0.69	4.21	0.95	2.56	0.39	2.37	0.37	2.84	1.02
XHH04	42.4	392	90.3	17.1	96.8	6.14	165	24.8	81	2.41	4.06	0.32	1.11	0.21	4.12	8.15	18.4	2.51	11.4	3.33	1.15	4.08	0.68	4.33	0.98	2.99	0.43	2.69	0.42	2.17	0.95
XHH05	42.2	428	90.2	17.4	69.6	3.72	146	27.9	90	2.52	3.71	0.31	1.29	0.27	3.14	8.93	20.2	2.81	12.4	3.71	1.32	4.57	0.76	4.86	1.11	3.17	0.48	3.02	0.45	2.12	0.98

Table 5
Sr-Nd isotopic compositions of representative samples in the study areas from the eastern NCC.

Sample	Rb (ppm)	Sr (ppm)	$^{87}Rb/^{86}Sr$	$^{87}Sr/^{86}Sr$	± 2s	Sm (ppm)	Nd (ppm)	$^{147}Sm/^{144}Nd$	$^{143}Nd/^{144}Nd$	± 2s	$(^{87}Sr/^{86}Sr)_i$	$(^{143}Nd/^{144}Nd)_i$	ε_{Nd} (t)
LWM01	22.3	252	0.2561	0.707239	0.000008	3.66	19.1	0.1154	0.512193	0.000005	0.706467	0.512033	-6.5
LWM02	33.5	242	0.4006	0.707402	0.000014	3.79	17.5	0.1304	0.512204	0.000009	0.706194	0.512023	-6.7
LWM03	17.7	271	0.1890	0.707064	0.000007	3.72	17.9	0.1251	0.512215	0.000013	0.706494	0.512041	-6.3
LWM06	6.02	242	0.0720	0.706440	0.000009	3.23	14.6	0.1332	0.512201	0.000005	0.706223	0.512016	-6.8
WJZ01	3.72	196	0.0549	0.706621	0.000009	2.42	10.5	0.1387	0.512192	0.000010	0.706466	0.512011	-7.2
WJZ03	3.56	183	0.0563	0.706621	0.000009	2.24	8.48	0.1590	0.512182	0.000010	0.706461	0.512003	-7.4
MJZ03	10.4	138	0.2189	0.707958	0.000009	2.55	8.04	0.1909	0.511576	0.000006	0.707417	0.511458	-19.6
MJZ04	9.51	133	0.2069	0.707861	0.000008	2.69	8.21	0.1972	0.511585	0.000005	0.707459	0.511473	-19.3
MJZ05	14.1	138	0.2957	0.707928	0.000013	2.54	8.52	0.1795	0.511589	0.000009	0.707355	0.511464	-19.5
MJZ11	33.4	135	0.7160	0.708671	0.000007	3.62	12.2	0.1786	0.511636	0.000006	0.707283	0.511512	-18.5
MJZ18	1.50	146	0.0298	0.707408	0.000010	3.80	12.6	0.1816	0.511636	0.000008	0.707350	0.511521	-18.4
MJZ25	1.61	155	0.0302	0.707623	0.000008	3.73	11.7	0.1919	0.511623	0.000006	0.707564	0.511509	-18.6
MJZ28	2.43	140	0.0504	0.707450	0.000007	3.69	11.9	0.1867	0.511625	0.000026	0.707353	0.511508	-18.6
MJZ36	2.11	133	0.0459	0.707429	0.000007	3.67	12.4	0.1782	0.511626	0.000007	0.707340	0.511510	-18.6
JY03	6.12	290	0.0611	0.706588	0.000007	4.49	18.0	0.1502	0.511829	0.000011	0.706469	0.511829	-15.7
JY07	1.91	308	0.0179	0.706364	0.000008	4.52	17.6	0.1546	0.511797	0.000011	0.706329	0.511797	-15.7
JY14	5.22	295	0.0512	0.706376	0.000010	4.53	19.2	0.1420	0.511771	0.000008	0.706277	0.511771	-16.0
JY15	4.04	204	0.0573	0.706407	0.000006	2.38	9.33	0.1536	0.511816	0.000007	0.706296	0.511816	-15.3
HM01	88.8	72.8	3.5300	0.711491	0.000010	27.3	116.5	0.1411	0.511654	0.000009	0.705295	0.511550	-18.1
HM03	93.5	72.9	3.7118	0.711870	0.000013	23.6	107	0.1328	0.511649	0.000008	0.705355	0.511541	-18.3
XHH02	22.4	135	0.4802	0.706049	0.000007	3.51	11.7	0.1806	0.511616	0.000006	0.705207	0.511546	-18.2
XHH03	4.32	305	0.0410	0.705432	0.000009	4.61	17.9	0.1550	0.511625	0.000006	0.705360	0.511554	-18.0
XHH04	6.14	165	0.1080	0.705398	0.000007	3.33	11.4	0.1758	0.511616	0.000006	0.705208	0.511544	-18.3
XHH05	3.72	146	0.0740	0.70527004	0.000006	3.71	12.4	0.1801	0.511653	0.000007	0.705140	0.511542	-18.3

123.3 ± 1.3 Ma (n = 11, MSWD = 0.72) (Fig. 3-2).

5.2. Whole-rock K-Ar Ages

The whole-rock K-Ar dating results are listed in Table 2. The results show that the six mafic dykes (LWM03: 215.3 ± 4.6 Ma, WJZ02: 204.5 ± 5.2 Ma, MJZ04: 138.2 ± 3.3 Ma, JY03: 137.4 ± 2.8 Ma, HM01: 125.3 ± 2.4 Ma, and XHH02:125.6 ± 2.7 Ma) ranging in age from 125.3 ± 2.4 Ma to 215.3 ± 4.6 Ma (Fig. 4), were emplaced between late Triassic and early Cretaceous.

5.3. Geochemistry

Longwanmio mafic dyes: The Longwangmiao dykes are sub-alkaline with relatively uniform major oxide, trace element and Sr-Nd-Pb-zircon Hf isotopic compositions (Fig. 4, 5, 6, 7, 8, 9, 10). These rocks have low silica (SiO_2 = 48.68-50.90 wt.%) and low alkalis ($Na_2O + K_2O$ = 4.13-5.25 wt.%), and plot in the field of alkaline (shoshonitic) series (Fig. 5a, b; Le Maitre et al., 1989). These mafic dykes are characterized by high MgO (> 6.0 wt.%; $Mg^{\#}$ > 60), Fe_2O_3, Cao, MnO, Pb and low in Rb, Sr and Th (Fig. 6b), with minor enrichment of LREE ($(La/Yb)_N$ = 4.38-5.97) and LILE (Ba and K), depletion of HFSE (Nb, Ta, P, Zr, Hf, and Ti) and Eu (Eu_N/Eu^* = 0.87-0.97) (Fig. 6b). All dykes from this region have high Sr, Pb and low Nd and zircon Hf isotopic ratios ($(^{87}Sr/^{86}Sr)_{i>}$ 0.706; ε_{Nd} (t) < −6.3, $(^{206}Pb/^{204}Pb)_i$ > 16.6, $(^{207}Pb/^{204}Pb)_{i>}$ 15.4, $(^{208}Pb/^{204}Pb)_{i>}$ 36.8, ε_{Hf} (t) < −22.4) (Table 5, 6, 7; Figs. 7, 8, 9, 10).

Sample	Study area	Rock type	Dating method	Age (Ma)
LWM03	Longwangmiao	dolerite	K-Ar	215.3
WJZ02	Weijiazhuang	dolerite	K-Ar	204.5
MJZ04	Mengjiazhuang	dolerite	K-Ar	138.2
Jy03	Jiayou	dolerite	K-Ar	137.4
Hm01	Huangmi	dolerite	K-Ar	125.3
XHH02	Xiahonghe	dolerite	K-Ar	125.6

Fig. 4. K-Ar age for the mafic dykes in the present study areas from the eastern NCC.

Weijiazhuang mafic dykes: The Weijiazhuang dykes are characterized by high MgO (MgO > 7.7 wt.%; $Mg^{\#}$ > 67), SiO_2 (> 47.6 wt.%), A_2O_3 (> 14.0 wt.%) and CaO (> 9.8 wt.%), and low TiO_2 (0.63-0.68 wt.%), Fe_2O_3 (10.38-10.87 wt.%), MnO (< 0.17 wt.%), P_2O_5 (< 0.16 wt.%), alkalis ($Na_2O + K_2O$ > 3.6 wt.%), Rb, Sr and Th (Tables 3, 4; Figs. 5, 6 b). These dykes belong to sub-alkaline (shoshonitic and calc-alkaline) series (Fig. 5a, b; Le Maitre et al., 1989). They show enrichment of LILE (Ba and K) and LREE ($(La/Yb)_{N>}$ 3.79-5.37) (Fig. 6a, b) and negative Eu (Eu_N/Eu^* = 0.89-0.97), Nb, Ta, P, Zr, Hf and Ti anomalies on spider diagram (Fig. 6a, b). In addition, the mafic dykes in this region display relatively high Sr, Pb and low Nd and zircon Hf isotopic ratios ($(^{87}Sr/^{86}Sr)_{i>}$ 0.706; ε_{Nd} (t) < −7.0, $(^{206}Pb/^{204}Pb)_i$ > 16.7, $(^{207}Pb/^{204}Pb)_{i>}$ 15.4, $(^{208}Pb/^{204}Pb)_{i>}$ 36.9, ε_{Hf} (t) < −23.3) (Tables 5, 6, 7; Figs. 7, 8, 9, 10).

Mengjiazhuang mafic dykes: The Mengjiazhuang dykes are shoshonitic and calc-alkaline with high SiO_2 (> 48.9 wt.%), TiO_2 (> 0.8 wt.%), Fe_2O_3 (> 13.6 wt.%), MnO (0.19-0.20 wt.%), MgO (MgO > 5.8 wt.%; $Mg^{\#}$ > 58), CaO (> 8.9 wt.%), alkalis ($Na_2O + K_2O$ > 3.3 wt.%), Rb, Sr, Th and low P_2O_5 (< 0.15 wt.%) (Tables 3, 4; Fig. 5 Figs. 5 a, b, 6 a, b).These dykes belong to sub-alkaline (shoshonitic) series (Fig. 5a, b; Le Maitre et al., 1989). Furthermore, the Mengjiazhuang dykes are characterized by enrichment in LILE (Ba and K) and LREE ($(La/Yb)_N$ = 2.44-2.91), depletion in Eu (Eu_N/Eu^* = 0.87-0.96), Nb, Ta, P, Zr, Hf and Ti on spider diagram (Fig. 6a, b). They also show high Sr, Pb and low Nd, zircon Hf isotopic ratios ($(^{87}Sr/^{86}Sr)_{i>}$ 0.706; ε_{Nd} (t) < −18.4, $(^{206}Pb/^{204}Pb)_i$ > 16.7, $(^{207}Pb/^{204}Pb)_{i>}$ 15.4, $(^{208}Pb/^{204}Pb)_{i>}$ 36.9, ε_{Hf} (t) < −8.6) (Tables 5, 6, 7; Figs. 7, 8, 9, 10).

5.4. Jiayou mafic dykes

These dykes show high SiO_2 (> 48.5 wt.%), TiO_2 (> 1.15 wt.% except JY15), A_2O_3 (> 13.9 wt.%), Fe_2O_3 (> 14.5 wt.% except JY15), MnO (0.19-0.25 wt.%), MgO (MgO > 6.0 wt.%; $Mg^{\#}$ > 59), CaO (> 9.0 wt.%), alkalis ($Na_2O + K_2O$ > 3.3 wt.%), P_2O_5 (> 0.18 wt.% except JY15), Rb, Sr and Th (Tables 3, 4; Figs. 5 a, b, 6 a, b). The Jiayou dykes belong to sub-alkaline (shoshonitic) series (Fig. 3a, b; Le Maitre et al., 1989). Moreover, the dykes from Jiayou also show enrichment in LILE (Ba and K) and LREE ($(La/Yb)_{N>}$ 3.7), depletion in Eu ($Eu_N/$

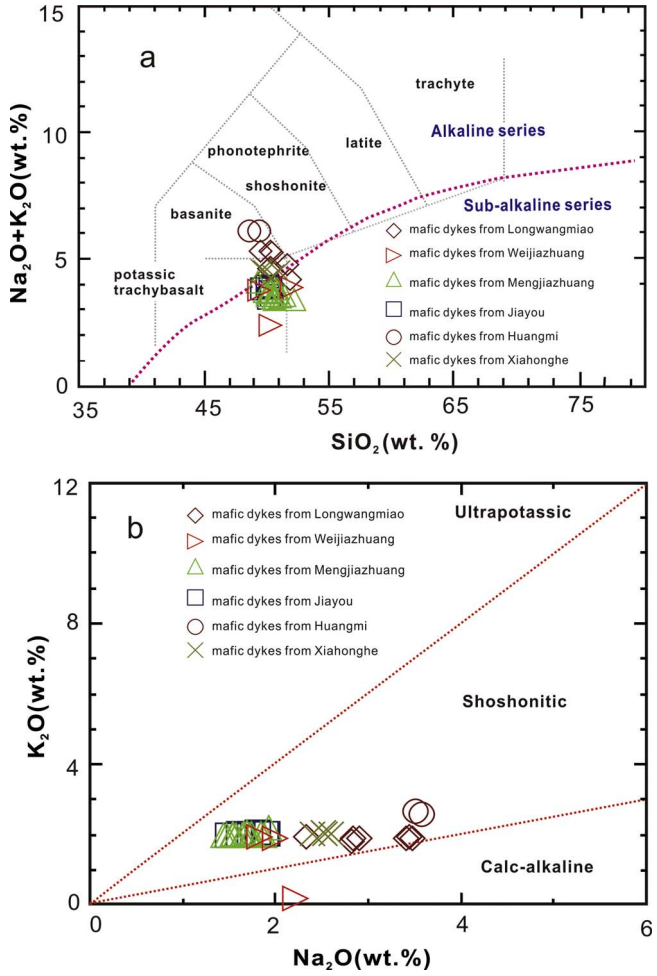

Fig. 5. Total alkali vs. silica (TAS) (a) and Na_2O vs. K_2O (b) plots for the mafic dykes within the study areas from the eastern NCC. All major element data have been re-calculated to 100% on an anhydrous basis (Middlemost, 1994; Le Maitre, 2002).

Eu* = 0.90-1.03 except JY14), Nb, Ta, P, Zr, Hf and Ti on spider diagram (Fig. 6a, b). They display high Sr, Pb and low Nd and zircon Hf isotopic ratios ($(^{87}Sr/^{86}Sr)_{i>}$ 0.706; $\varepsilon_{Nd}(t) < -15.3$, $(^{206}Pb/^{204}Pb)_{i} > 16.7$, $(^{207}Pb/^{204}Pb)_{i>}$ 15.4, $(^{208}Pb/^{204}Pb)_{i>}$ 36.9, $\varepsilon_{Hf}(t) < -18.4$) (Tables 5, 6, 7; Figs. 7, 8, 9, 10).

5.5. Huangmi mafic dykes

The Huangmi dykes have high TiO_2 (> 2.7 wt.%), A_2O_3 (> 17.2 wt.%), MgO (MgO > 6.5 wt.%; $Mg^{\#}$ > 54), alkalis ($Na_2O + K_2O$ > 5.9 wt.%), P_2O_5 (> 1.05 wt.%), Rb, Sr and Th and low SiO_2 (< 48.0 wt.%), Fe_2O_3 (< 12.2 wt.%), MnO (0.03 wt.%), CaO (< 1.7 wt.%), (Tables 3, 4; Figs. 5 a, b, 6 a, b). The Huangmi dykes belong to alkaline (shoshonitic) series (Fig. 5a, b; Le Maitre et al., 1989). They display enrichment in LILE (Ba and K) and LREE ($(La/Yb)_N$ = 9.37-9.97), depletion in Eu (Eu_N/Eu^* = 0.83-0.86), Nb, Ta, P, Zr, Hf and Ti on spider diagram (Fig. 6a, b). These dykes possess high Sr, Pb and low Nd and zircon Hf isotopic ratios ($(^{87}Sr/^{86}Sr)_{i>}$ 0.705; $\varepsilon_{Nd}(t) < -15.1$, $(^{206}Pb/^{204}Pb)_{i} > 16.9$, $(^{207}Pb/^{204}Pb)_{i>}$ 15.5, $(^{208}Pb/^{204}Pb)_{i>}$ 36.9, $\varepsilon_{Hf}(t) < -12.2$) (Table 5, 6, 7; Figs. 7, 8, 9, 10).

Xiahonghe mafic dykes: These dykes are characterized by enrichment of SiO_2 (> 48.4 wt.%), Fe_2O_3 (> 13.8 wt.%), MnO (> 0.19 wt.%), MgO (MgO > 5.6 wt.%; $Mg^{\#}$ > 60), CaO (> 9.4 wt.%), alkalis ($Na_2O + K_2O$ > 4.3 wt.%), Rb, Sr and Th (Tables 3, 4; Figs. 5 a, b, 6 a, b), and depletion of TiO_2 (< 1.3 wt.%), A_2O_3 (< 14.5 wt.%), P_2O_5 (< 0.14 wt.% except XHH03). The Xiahonghe dykes belong to alkaline (shoshonitic) series (Fig. 5a, b; Le Maitre et al., 1989). In addition, they also show enrichment in LILE (Ba and K) and LREE ($(La/Yb)_N$ = 2.12-2.84), depletion in Eu (Eu_N/Eu^* = 0.82-1.02 except XHH03), Nb, Ta, Zr, Hf and Ti on spider diagram (Fig. 6a, b). They possess high Sr, Pb and low Nd and zircon Hf isotopic ratios ($(^{87}Sr/^{86}Sr)_{i>}$ 0.705; $\varepsilon_{Nd}(t) < -18.0$, $(^{206}Pb/^{204}Pb)_{i} > 16.9$, $(^{207}Pb/^{204}Pb)_{i>}$ 15.5, $(^{208}Pb/^{204}Pb)_{i>}$ 36.9, $\varepsilon_{Hf}(t) < -8.6$) (Tables 5, 6, 7; Figs. 7, 8, 9, 10).

6. Discussion

6.1. Nature of the source and degree of melting

The studied mafic dykes show lower SiO_2 (< −51.57 wt.%) (Table 3) than liquids produced from partial melting of any of the crustal rocks present in the area (e.g., granitoids; Rapp et al., 2003; Hirajima et al., 1990; Zhang et al., 1995; Kato et al., 1997; Gao et al., 1998a,b), suggesting that these rocks formed from a mantle-derived component rather than a crustal source. This is also supported by high

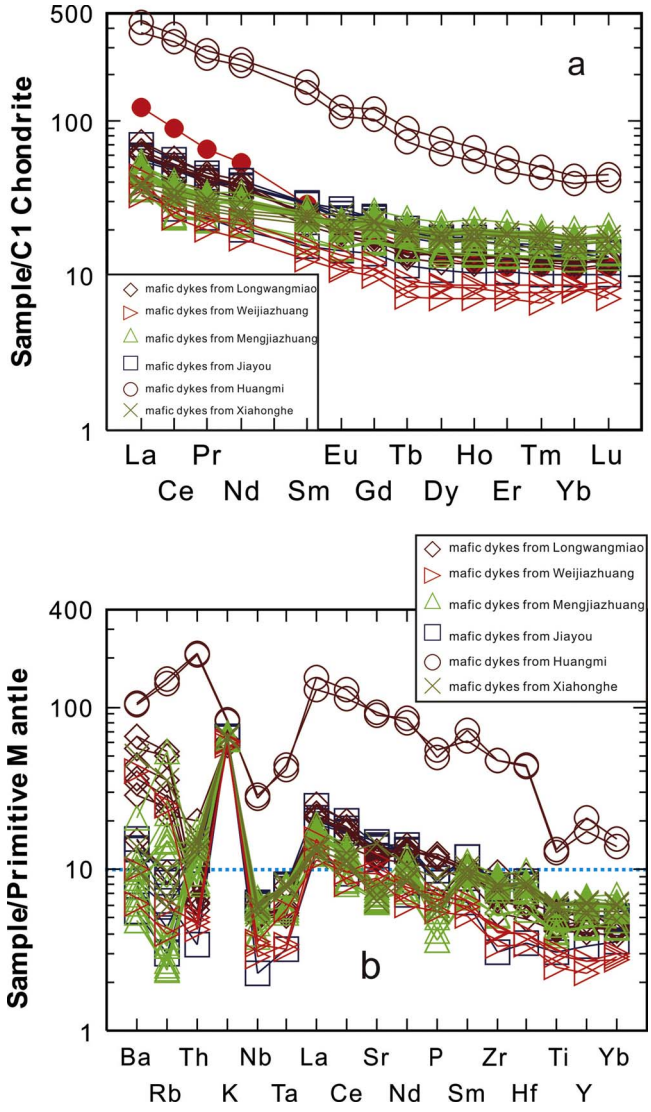

Fig. 6. Chondrite-normalized REE (a) and primitive-mantle-normalized (b) multi-element variation diagrams of the mafic dykes in the study areasfrom the eastern NCC. The values are normalized to the chondrite and primitive mantle compositions of Sun and McDonough (1989).

Table 6
Pb isotopic compositions of representative samples in the study areas from the eastern NCC.

Sample	Age (Ma)	$^{206}Pb/^{204}Pb$	$^{207}Pb/^{204}Pb$	$^{208}Pb/^{204}Pb$	U (ppm)	Pb (ppm)	Th (ppm)	$(^{206}Pb/^{204}Pb)_i$	$(^{207}Pb/^{204}Pb)_i$	$(^{208}Pb/^{204}Pb)_i$
LWM01	212	16.812	15.463	37.034	1.56	46.3	8.21	16.744	15.460	36.917
LWM02	212	16.805	15.462	37.031	1.52	21.4	4.62	16.661	15.455	36.888
LWM03	212	16.861	15.458	37.033	1.54	20.8	4.58	16.711	15.450	36.887
LWM06	212	16.793	15.448	37.001	1.18	37.3	4.12	16.729	15.445	36.928
WJZ01	199.6	16.785	15.441	37.002	1.23	36.1	4.04	16.720	15.438	36.932
WJZ03	199.6	16.794	15.443	37.004	1.24	33.2	3.92	16.723	15.439	36.931
MJZ03	136.4	16.804	15.439	37.203	1.11	18.5	11.7	16.726	15.435	36.934
MJZ04	136.4	16.812	15.438	37.202	1.23	18.4	11.5	16.725	15.434	36.936
MJZ05	136.4	16.883	15.443	37.194	1.95	16.2	9.75	16.726	15.435	36.937
MJZ11	136.4	16.789	15.439	37.086	2.12	43.6	15.4	16.726	15.436	36.936
MJZ18	136.4	16.791	15.437	37.082	2.24	45.4	15.5	16.727	15.434	36.937
MJZ25	136.4	16.791	15.439	37.061	2.16	44.3	13.2	16.728	15.436	36.934
MJZ28	136.4	16.768	15.437	37.015	1.48	45.5	8.31	16.726	15.435	36.937
MJZ36	136.4	16.836	15.442	37.037	1.62	18.7	4.53	16.723	15.437	36.934
JY03	136.4	16.766	15.436	37.014	1.43	43.6	8.14	16.723	15.434	36.935
JY07	136.4	16.793	15.439	37.058	2.28	44.3	12.7	16.726	15.436	36.936
JY14	136.4	16.812	15.438	37.055	2.52	37.6	10.6	16.725	15.434	36.935
JY15	136.4	16.865	15.443	37.159	2.31	21.8	11.5	16.727	15.436	36.934
HM01	123.5	17.063	15.534	37.056	0.92	15.6	5.43	16.993	15.531	36.921
HM03	123.5	17.041	15.531	37.184	0.75	19.2	13.1	16.995	15.529	36.920
XHH02	123.3	17.048	15.534	36.993	1.21	26.2	4.78	16.994	15.531	36.923
XHH03	123.3	17.063	15.535	37.077	3.45	57.8	23.3	16.993	15.532	36.921
XHH04	123.3	17.067	15.538	37.064	3.38	55.4	20.5	16.995	15.535	36.921
XHH05	123.3	17.061	15.536	37.086	3.66	64.6	27.2	16.994	15.533	36.923

MgO (5.68-11.11 wt.%), $Mg^{\#}$ (54-68) and Cr contents (80.1–770 ppm) in the mafic dykes. In addition, the high initial $^{87}Sr/^{86}Sr$ ratios (> 0.705), $(^{206}Pb/^{204}Pb)_i$ (> 16.661), $(^{207}Pb/^{204}Pb)_i$ (> 15.434) and $(^{208}Pb/^{204}Pb)_i$ (> 36.887) ratios, and negative ε_{Nd} (t) (from −6.3 to −19.6) and zircon ε_{Hf} (t) (from −8.4 to −23.9) values (Tables 4, 5, 6; Fig. 7, 8, 9, 10) for the dykes are consistent with derivation from partial melting of an enriched lithospheric mantle source (EM1-like; Fig. 7) beneath the NCC, rather than an asthenospheric mantle source with a depleted Sr-Nd isotopic composition, such as mid-ocean ridge basalt (Liu et al., 2009a,b). Plots of La/Sm vs. La and Sm/Yb vs. Sm (Fig. 11a, b) suggest that the magma for these dykes were possibly sourced from garnet-lherzolite (Longwangmiao, Weijiazhuang, and Jiayou) and spinel-lherzolite (Mengjiazhuang, Huangmi, and Xiahonghe)mantle through moderate degree of partial melting (10%-30%). In primitive mantle normalized spider diagrams (Fig. 6b), all dykes reveal very distinctive negative anomalies for Nb, Ta, and Ti, and positive anomalies for Pb. The HFSE-depletion indicates the involvement of components from the proto-Tethyan oceanic or ancient continental crust (Zhang et al., 2005a,b). Moreover, the relatively uniform La/Nb ratios (2-5) and higher Ba/Nb (8-137) in the studied dykes differ from those of most intra-plate volcanic rocks (N-MORB, OIB, alkali basalts and kimberlites) with lower La/Nb and Ba/Nb ratios (0.5-2.5, and 1-20) (Table 4). Accordingly, we infer that continental materials were involved in these mantle-derived magmas (Jahn et al., 1999).

6.2. Fractional crystallization

The mafic dykes crystallized from a fractionated mafic magma as evidenced by high MgO (5.68-11.11 wt.%), $Mg^{\#}$ (54-68) (Table 3) and compatible elements, such as Cr (80.1–770 ppm) contents (Table 4). The fractional crystallization trends during magma evolution can be shown on MgO vs. $(^{87}Sr/^{86}Sr)_i$, ε_{Nd} (t) and $(^{206}Pb/^{204}Pb)_i$ correlative plots (Fig. 12a–c). No obvious correlation exists between MgO and SiO_2, TiO_2, Al_2O_3, Fe_2O_3, CaO, Na_2O, P_2O_5, Sr and Zr (figure not presented), suggesting inconspicuous fractionation of olivine, clinopyroxene and hornblende. The crystal fractionation of rutile also can be ruled out, as fractionation of even low amounts of rutile would produce elevated Nb/Ta ratio with strongly decreasing Nb (JÖrg et al., 2007), which is not observed. However, the separation of plagioclase, Ti-bearing oxides and apatite might account for the observed negative Eu, Sr, Nb, Ta, Ti anomalies in the chondrite-normalized REE pattern and primitive mantle-normalized spider diagrams (Fig. 6a, b). Furthermore, plots of Sr vs. Ba and Rb (not presented), suggest fractionation of plagioclase in the parental magmas.

6.3. Crustal contamination

Since the studied mafic dykes were emplaced within a continental setting, it is possible that the mafic mantle-derived magmas experienced some degree of crustal contamination during ascent and/or residence within crustal magma chambers (Mohr, 1987). It is necessary, therefore, to evaluate the extent of crustal contamination. Geochemical characteristics, including significant depletion in Nb-Ta, high initial Sr isotopic composition and negative ε_{Nd} (t) and ε_{Hf} (t) values, suggest the involvement of continental crustal component in the magma genesis of the mafic dykes (Guo et al., 2013). Such continental signature can be introduced by contamination during magma ascent or may also reflect the character of a metasomatized mantle source. The mafic dykes are characterized by depletion in Th relative to La (Fig. 6b), eliminating the possibility of significant upper-middle crustal contamination (Taylor and McLennan, 1985). Therefore, a likely candidate for the contamination might be lower crust. Nevertheless, as shown in Fig. 12, crustal assimilation is not supported. The lack of correlations between MgO and initial $^{87}Sr/^{86}Sr$ ratios and ε_{Nd} (t) values (Fig. 12a, b) also preclude any extensive crustal contamination. In summary, we infer that magma evolution of the mafic dykes was not significantly affected by crustal contamination and therefore the geochemical and isotopic signatures of these dykes were mainly inherited from the enriched mantle source.

6.4. Mantle metasomatism

As mentioned in the previous section, continental materials were involved in the formation of the mantle-derived parental magmas of the mafic dykes. Volatile-bearing minerals (amphibole, mica and apatite) may play a major role in creating lithospheric sources enriched in incompatible lithophile elements. In general, phlogopite has a high Rb/Sr ratio (0.13-60) (Lonov et al., 1997) and as such our data (Table 4) suggest that both phlogopite and amphibole are essential components in lithospheric mantle domains beneath the study area. The high Rb/Sr

Table 7
Hf isotopic compositions of representative samples in the study areas from the eastern NCC.

LWM01								
Spot	$^{176}Yb/^{177}Hf$	$^{176}Lu/^{177}Hf$	$^{176}Hf/^{177}Hf$	2s	ε_{Hf} (t)	T_{DM1} (Ma)	T_{DM2} (Ma)	$f_{Lu/Hf}$
1	0.027346	0.000793	0.282007	0.000028	-22.5	1744	2663	-0.98
2	0.036873	0.001103	0.282001	0.000035	-22.8	1766	2678	-0.97
3	0.048876	0.001308	0.282002	0.000020	-22.8	1775	2679	-0.96
4	0.018427	0.000554	0.282008	0.000063	-22.5	1731	2659	-0.98
5	0.054608	0.001572	0.282001	0.000036	-22.8	1788	2682	-0.95
6	0.036305	0.001061	0.282001	0.000026	-22.8	1764	2677	-0.97
7	0.036916	0.001040	0.282003	0.000021	-22.7	1761	2674	-0.97
8	0.068892	0.001927	0.282004	0.000040	-22.8	1801	2679	-0.94
9	0.023998	0.000726	0.282013	0.000041	-22.3	1732	2649	-0.98
10	0.060865	0.001697	0.282013	0.000033	-22.4	1777	2656	-0.95
11	0.017414	0.000502	0.282001	0.000022	-22.7	1738	2673	-0.98
12	0.046212	0.001307	0.282002	0.000029	-22.8	1775	2678	-0.96
13	0.044853	0.001340	0.282005	0.000042	-22.7	1772	2672	-0.96
14	0.044956	0.001319	0.282002	0.000028	-22.8	1775	2679	-0.96
15	0.017467	0.000467	0.282003	0.000020	-22.6	1734	2669	-0.99
16	0.056231	0.001475	0.282002	0.000025	-22.8	1783	2680	-0.96
–								
WJZ03								
Spot	$^{176}Yb/^{177}Hf$	$^{176}Lu/^{177}Hf$	$^{176}Hf/^{177}Hf$	2s	ε_{Hf} (t)	T_{DM1} (Ma)	T_{DM2} (Ma)	$f_{Lu/Hf}$
1	0.056223	0.001564	0.282022	0.000026	-23.9	1758	2686	-0.95
2	0.058063	0.001597	0.282033	0.000028	-23.5	1744	2661	-0.95
3	0.042811	0.001205	0.282032	0.000022	-23.6	1728	2663	-0.96
4	0.043577	0.001298	0.282022	0.000040	-23.9	1746	2685	-0.96
5	0.055136	0.001480	0.282013	0.000026	-24.2	1766	2705	-0.96
6	0.036298	0.000977	0.282029	0.000036	-23.7	1721	2668	-0.97
7	0.044768	0.001284	0.282011	0.000028	-24.3	1761	2710	-0.96
8	0.053141	0.001498	0.282026	0.000034	-23.8	1750	2678	-0.95
9	0.054477	0.001415	0.282036	0.000022	-23.4	1732	2655	-0.96
10	0.037234	0.000992	0.282039	0.000022	-23.3	1709	2647	-0.97
11	0.047833	0.001387	0.282011	0.000024	-24.3	1766	2710	-0.96
12	0.045224	0.001317	0.282028	0.000029	-23.7	1739	2673	-0.96
13	0.027634	0.000771	0.282020	0.000023	-23.9	1724	2687	-0.98
14	0.038287	0.001160	0.282039	0.000024	-23.3	1716	2647	-0.97
15	0.040082	0.001053	0.282036	0.000024	-23.4	1716	2654	-0.97
16	0.055065	0.001477	0.282035	0.000026	-23.5	1736	2657	-0.96
–								
MJZ02								
Spot	$^{176}Yb/^{177}Hf$	$^{176}Lu/^{177}Hf$	$^{176}Hf/^{177}Hf$	2s	ε_{Hf} (t)	T_{DM1} (Ma)	T_{DM2} (Ma)	$f_{Lu/Hf}$
1	0.072442	0.002053	0.282447	0.000019	-8.7	1172	1738	-0.94
2	0.056303	0.001735	0.282441	0.000020	-8.9	1170	1749	-0.95
3	0.051207	0.001744	0.282445	0.000058	-8.7	1165	1740	-0.95
4	0.069735	0.002062	0.282443	0.000019	-8.8	1178	1745	-0.94
5	0.023131	0.001082	0.282410	0.000038	-9.8	1193	1812	-0.97
6	0.085032	0.002603	0.282446	0.000028	-8.7	1191	1741	-0.92
7	0.086050	0.002622	0.282381	0.000023	-11.0	1287	1885	-0.92
8	0.035603	0.001101	0.282437	0.000049	-8.8	1156	1751	-0.97
9	0.054731	0.001659	0.282395	0.000044	-10.3	1233	1846	-0.95
10	0.085644	0.003186	0.282440	0.000061	-8.8	1219	1754	-0.90
11	0.034732	0.000897	0.282436	0.000023	-8.8	1151	1749	-0.97
12	0.034649	0.001322	0.282446	0.000023	-8.4	1151	1731	-0.96
13	0.034146	0.001076	0.282438	0.000027	-8.7	1154	1746	-0.97
14	0.054736	0.001722	0.282396	0.000026	-10.2	1234	1842	-0.95
15	0.024197	0.001091	0.282413	0.000022	-9.5	1190	1801	-0.97
16	0.035610	0.001104	0.282435	0.000051	-8.7	1159	1750	-0.97
17	0.034268	0.001106	0.282437	0.000048	-8.6	1157	1746	-0.97
–								
YJ01								
Spot	$^{176}Yb/^{177}Hf$	$^{176}Lu/^{177}Hf$	$^{176}Hf/^{177}Hf$	2s	ε_{Hf} (t)	T_{DM1} (Ma)	T_{DM2} (Ma)	$f_{Lu/Hf}$
1	0.001808	0.000835	0.282128	0.000024	-19.9	1578	2441	-0.97
2	0.001967	0.000827	0.282119	0.000019	-20.2	1590	2461	-0.98
3	0.002210	0.000731	0.282121	0.000044	-20.1	1583	2456	-0.98
4	0.001890	0.000901	0.282123	0.000028	-20.0	1588	2452	-0.97
5	0.001532	0.000679	0.282109	0.000022	-20.5	1598	2483	-0.98
6	0.004109	0.000724	0.282143	0.000036	-19.3	1553	2407	-0.98
7	0.003520	0.000557	0.282112	0.000022	-20.4	1589	2475	-0.98
8	0.004399	0.000725	0.282136	0.000022	-19.6	1562	2422	-0.98
9	0.004735	0.000648	0.282149	0.000030	-19.1	1542	2393	-0.98
10	0.006154	0.000481	0.282140	0.000034	-19.4	1547	2412	-0.99
11	0.003495	0.000717	0.282142	0.000037	-19.4	1554	2409	-0.98
12	0.002997	0.000810	0.282130	0.000059	-19.8	1574	2436	-0.98
13	0.006720	0.000494	0.282149	0.000037	-19.1	1536	2393	-0.99
14	0.003042	0.000726	0.282138	0.000025	-19.5	1560	2419	-0.98
15	0.005032	0.000731	0.282170	0.000032	-18.4	1516	2348	-0.98

(*continued on next page*)

Table 7 (*continued*)

LWM01								
16	0.002082	0.000775	0.282139	0.000039	-19.5	1560	2416	-0.98
–								
HM03								
Spot	$^{176}Yb/^{177}Hf$	$^{176}Lu/^{177}Hf$	$^{176}Hf/^{177}Hf$	2s	ε_{Hf} (t)	T_{DM1} (Ma)	T_{DM2} (Ma)	$f_{Lu/Hf}$
1	0.024835	0.000763	0.282272	0.000035	-13.4	1376	2083	-0.98
2	0.033430	0.001064	0.282262	0.000045	-13.8	1401	2108	-0.97
3	0.042486	0.001254	0.282265	0.000050	-13.7	1403	2102	-0.96
4	0.024181	0.000643	0.282304	0.000027	-12.3	1327	2011	-0.98
5	0.018763	0.000579	0.282258	0.000026	-13.9	1389	2113	-0.98
6	0.013162	0.000364	0.282304	0.000020	-12.2	1317	2008	-0.99
7	0.009441	0.000230	0.282269	0.000035	-13.5	1361	2086	-0.99
8	0.014967	0.000321	0.282242	0.000022	-14.4	1401	2146	-0.99
9	0.028467	0.000834	0.282277	0.000031	-13.2	1371	2072	-0.97
10	0.042885	0.001229	0.282319	0.000025	-11.8	1327	1983	-0.96
11	0.051710	0.001434	0.282258	0.000022	-14.0	1420	2118	-0.96
12	0.026722	0.000802	0.282256	0.000050	-14.0	1399	2118	-0.98
13	0.028310	0.000782	0.282295	0.000044	-12.6	1345	2033	-0.98
14	0.022850	0.000616	0.282306	0.000029	-12.2	1324	2007	-0.98
15	0.033056	0.001046	0.282259	0.000044	-13.9	1404	2113	-0.97
16	0.015541	0.000538	0.282301	0.000030	-12.4	1327	2016	-0.98
–								
XHH01								
Spot	$^{176}Yb/^{177}Hf$	$^{176}Lu/^{177}Hf$	$^{176}Hf/^{177}Hf$	2s	ε_{Hf} (t)	T_{DM1} (Ma)	T_{DM2} (Ma)	$f_{Lu/Hf}$
1	0.076671	0.002213	0.282418	0.000057	-10.0	1219	1810	-0.93
2	0.076673	0.002215	0.282417	0.000061	-10.0	1221	1813	-0.93
3	0.056360	0.001714	0.282453	0.000046	-8.7	1152	1729	-0.95
4	0.056345	0.001716	0.282456	0.000032	-8.6	1149	1723	-0.95
5	0.088837	0.002564	0.282379	0.000033	-11.3	1288	1898	-0.92
6	0.048712	0.001497	0.282345	0.000020	-12.4	1299	1967	-0.95
7	0.048703	0.001514	0.282348	0.000031	-12.3	1295	1960	-0.95
8	0.047506	0.001798	0.282443	0.000031	-8.9	1169	1749	-0.95
9	0.130991	0.003751	0.282409	0.000026	-10.3	1286	1834	-0.89
10	0.048118	0.001804	0.282441	0.000023	-9.0	1172	1752	-0.95
11	0.048228	0.001790	0.282437	0.000039	-9.1	1177	1760	-0.95
12	0.047550	0.001812	0.282429	0.000028	-9.3	1189	1777	-0.95
13	0.051707	0.001704	0.282439	0.000048	-9.0	1172	1754	-0.95
14	0.048218	0.001785	0.282434	0.000024	-9.1	1182	1765	-0.95
15	0.047505	0.001795	0.282445	0.000027	-8.7	1166	1740	-0.95
16	0.051696	0.001687	0.282436	0.000034	-9.0	1176	1759	-0.95

ratios (> 0.03) in the mafic dykes from Longwangmiao, Weijiazhuang, Mengjiazhuang, and Huangmi areas, however, indicate a predominance of phlogopite rather than amphibole in the melt source. Since Nb and Ta together with Zr and Hf display similar geochemical behavior (Jochum et al., 1989), the Nb/Ta and Zr/Hf ratios trace an unusual metasomatic assemblage during the formation of the mantle source (Guo et al., 2004; Liu et al., 2008a,c). It has been suggested that rutile is the major phase to produce superchondritic Nb/Ta ratios in the melts whereas low-Mg amphibole is the dominant phase to generate low Nb/Ta and high Zr/Hf ratios in the melts (Rudnick et al., 2000). In this case, the subchondritic Nb/Ta ratios (11-19) (Table 4) in the studied dykes suggest the possibility of low-Mg amphibole metasomatism in the source. Similarly, Zr/Hf ratio remains constant during petrogenetic processes with perhaps the exception of fluid-related metasomatism (Rudnick et al., 1993), crystallization of clinopyroxene (Beier et al., 2006), or fractionation of minor amounts of Ti-bearing phases (rutile, ilmenite, titanite) (JÖrg et al., 2007). The superchondritic Zr/Hf ratios (32-42) (chondritic ratio: 34.3 ± 0.3, MÜnker et al., 2003), might indicate small-volume carbonatite and low-Mg amphibole metasomatism in the mantle source (Rudnick et al., 1993; rg et al., 2007,c; Liu et al., 2008a,c), together with extensive fractionation of clinopyroxene, rutile and ilmenite. Furthermore, the studied dykes show significant enrichment in REE relative to HFSE (Fig. 6b). All of these features are characteristic of carbonatite metasomatism (Rudnick et al., 1993) and suggest that the source region for the mafic dykes has been metasomatised by carbonate-rich magmas or fluids (Liu et al., 2008a,c).

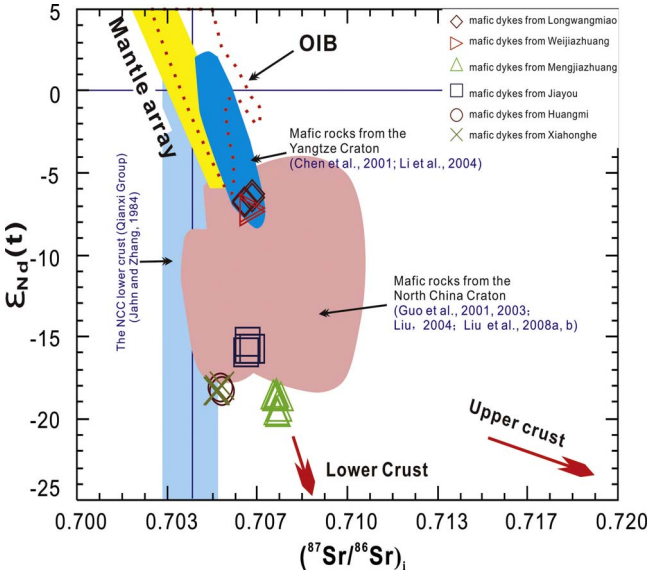

Fig. 7. Initial $^{87}Sr/^{86}Sr$ vs. ε_{Nd} (t) diagram for the mafic dykes in the study areas from the eastern NCC. Also shown are the compositions of Mesozoic mafic rocks from the NCC (Liu et al., 2008a,b,c) and the mafic rocks from the Yangtze Craton (Chen et al., 2001; Li et al., 2004).

In general, hybridization not only affects the original geochemical composition of peridotite, but also alters the geochemical nature of the newly generated igneous rock. Therefore, this process has potential influence on the abundance of elements in peridotite, i.e., the content of Nb, Zr, Hf, Y, Ti, Ga, Co and light rare earth elements will decrease

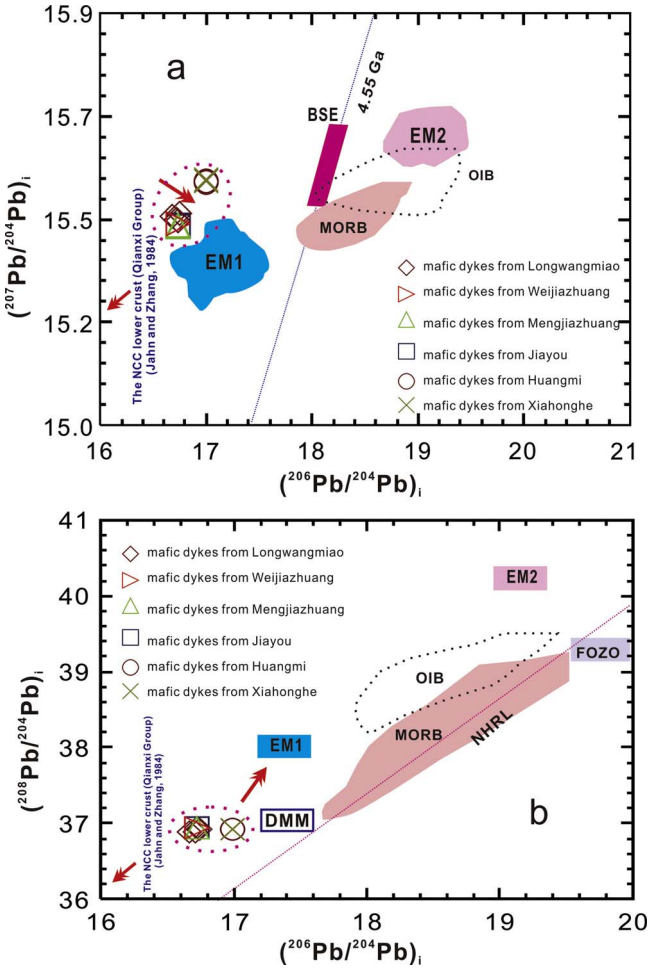

Fig. 8. $^{207}Pb/^{204}Pb$ (a) and $^{208}Pb/^{204}Pb$ (b) vs. $^{206}Pb/^{204}Pb$ diagrams for the mafic dykes in the study areas from the eastern NCC. Also shown are MORB, OIB, and NHRL fields after Barry and Zou et al. (2000), and a 4.55 Ga geochron from Hart (1984). EM1 and EM2 after Liu et al. (2008a,b, 2009). The NCC lower crust after Jahn and Zhang (1984).

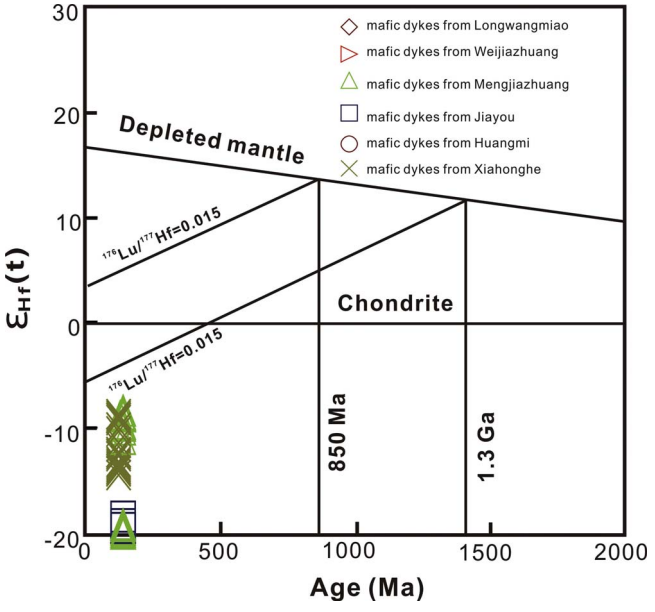

Fig. 9. Diagram of ages vs. ε_{Hf} (t) values from zircons (LWM01, WJZ03, MJZ02, JY01, HM03, and XHH01) from the mafic dykes in study areas from the eastern NCC.

gradually, in contrast, the content of heavy rare earth elements (Dy-Lu), Ba, Rb, K, Sr, Sc, Sr-Nd-Pb-Hf isotopes and Ni will increase gradually (Roden and Murthy, 1985; Hartrnann and Wedepohl, 1990). This would explain the composition characteristics of the mafic dykes including their geochemical and isotopic variations.

6.5. Genetic model

Based on the discussion in the previous section, the mafic dykes in the study are considered to have been derived from partial melting of an enriched mantle source (EM1-like; Fig. 8). Among the various mechanisms proposed for the formation of the enriched mantle source are the following. (1) The enriched mantle beneath eastern NCC was formed by addition of melts and/or fluids liberated from the subducted Yangtze crust (). (2) The melts from subducted ancient Pacific plate (Izanagi plate) metastasized and modified the lithospheric mantle beneath eastern NCC (e.g., Chen et al., 2004a). (3) Mantle plume (Yuan, 1996; Lu et al., 2000; Wu et al., 2008). (4) Lithospheric mantle beneath eastern NCC was progressively enriched due to successive hybridization of the foundered lower crust (e.g., Liu et al., 2008a,b,c). The studied mafic dykes have Pb isotopic characteristics (Table 5) that are distinct from those of the Yangtze Craton lithosphere (Yan et al., 2003; Fig. 6), excludes any involvement of Yangtze Craton lithosphere (Xie et al., 2006) in their genesis, which is further supported by the results of C-O stable isotopes on the high pressure-ultra high pressure rocks in the Dabie-Sulu belt (Zheng et al., 2003; Zheng et al., 2005). In contrast, the distinctive Pb isotopic data suggest that the mafic dykes were derived from the overlying NCC during the Mesozoic (Xie et al., 2006; Fig. 8). Additionally, it is generally believed that the subduction of the Yangtze Craton has little influence on the origin of the mafic dykes from this region (Zhang et al., 2002). Accordingly, the enriched mantle beneath the NCC cannot have formed by addition of melts or melts and fluids from the subducting Yangtze crust. The long-lasting subduction of the Pacific plate might have released melts and fluids into the surrounding mantle. However, evidence is scarce related to contribution of the Paleo-Pacific plate to the Mesozoic magmatism of eastern NCC and southern China (Zhang et al., 2005a,b; Yuan, 2007). Furthermore, some studies also indicate that the origin of the enriched lithospheric mantle sources for Mesozoic mantle-derived rocks from western NCC was unrelated to the subduction of Paleo-Pacific plate (Wang et al., 2006; Ying et al., 2007). Some workers have also proposed the influence of mantle plume (Yuan, 1996, 2007; Lu et al., 2000; Wilde et al., 2003; Hong et al., 2003; Zhao et al., 2004; Yan et al., 2007; Gao et al., 2012; Wen et al., 2016). However, there is no robust evidence from petrology, geochemistry or geophysical data for the existence of a mantle plume beneath this craton since Paleozoic (Guo et al., 2001a,b,c; Wu et al., 2008). Since the possibility of significant crustal assimilation during the ascent and emplacement of the mafic magmas has been eliminated, we need to evaluate the involvement of crustal components in the mantle source. Since eclogitic lower continental crust has higher density than that of lithospheric mantle peridotite by 0.2-0.4 gcm^{-3} (Rudnick and Fountain, 1995; Jull and Kelemen, 2001; Levander et al., 2006; Anderson, 2006), the foundering of eclogitic lower crust is most likely in collisional orogens which have undergone crustal thickening. Eclogites have lower melting temperatures than mantle peridotites (Yaxley, 2000; Kogiso et al., 2003; Sobolev et al., 2005), and can be recycled into the mantle (Kay and Kay, 1991; Jull and Kelemen, 2001; Gao et al., 2004). In general, eclogites can melt to produce silicic melts (tonalite to trondhjemite) that may variably hybridize the overlying mantle peridotite, producing olivine-free pyroxenite, and with further melting, basalt (Kogiso et al., 2003; Sobolev et al., 2005; Herzberg et al., 2007; Gao et al., 2008). The delamination model is further supported by the intense lithospheric thinning (Liu et al., 2008a,b,c), voluminous coeval magmatism (250-114Ma) (Chen et al., 2004; Wang et al., 2007a,b; Li et al., 2015; Xu et al., 2016), large-scale mineralization (Zhang et al., 1996; Ma, 1997; Tong, 2016) and the adakitic rocks observed in

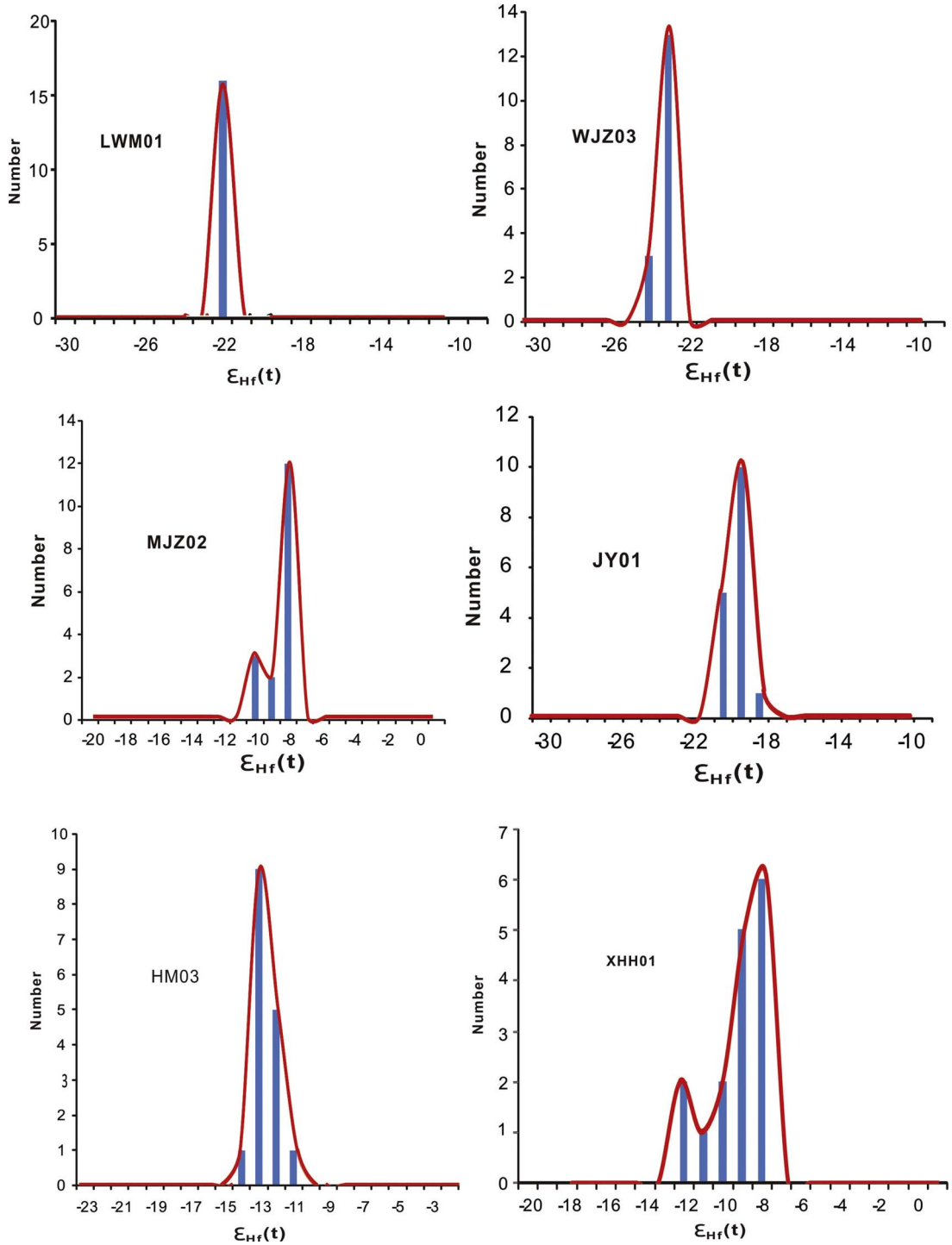

Fig. 10. Histograms of ε_{Hf} (t) values for the mafic dykes in the study areas from the eastern NCC.

adjacent areas (Davis, 2003; Hong et al., 2003,b; Zhang et al., 2005a,b; Dai et al., 2010; Tian, 2015; Xiao, 2016), which can all be explained through lithospheric foundering. We therefore suggest a model in which lower crustal delamination coincided with mafic magmatism (Fig. 13). During late Triassic (~240 Ma) (Zhang et al., 2005a,b; Liu et al., 2008a,b,c), the collision between the NCC and Yangtze Craton resulted in the formation of a thickened crust (Fig. 13a) and eclogitization of the lower domains of this crust (Qianxi Group, Li, 2007) beneath the study areas (Liu et al., 2008a,b,c). Subsequently (240-212 Ma), foundering of eclogite from the thickened lower crust (Fig. 13b) (Li et al., 2002; Liu et al., 2008a,b,c) triggered asthenospheric upwelling, uplift of eastern NCC, lithospheric extension and thinning. Silicic melts were generated by the extensive interaction of foundered eclogites and overlying mantle peridotite (metasomatic evidence from phlogopite, low-Mg amphibole and carbonate-rich magmas or fluids; Fig. 13c). Between late Triassic and Cretaceous (212-123 Ma), decompressional melting of the hybridized lithospheric mantle produced the primary magma (basaltic melts), that underwent fractionation of plagioclase, Ti-bearing oxides and apatite to produce mafic dyke swarms in the study area, with negligible crustal contamination.

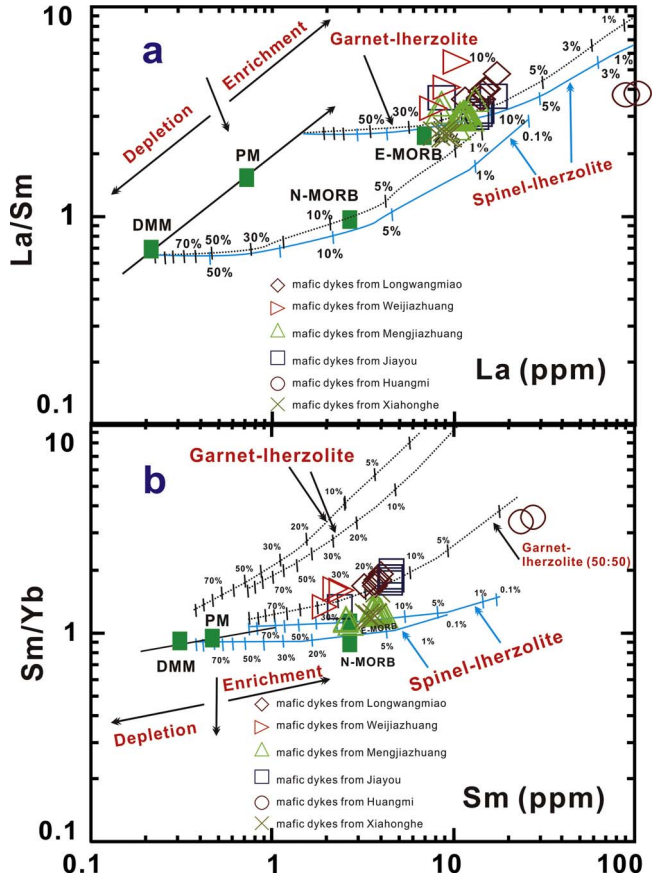

Fig. 11. La vs. La/Sm (a) and Sm vs. Sm/Yb diagrams for the mafic dykes in the study areas from the eastern NCC (Liu et al., 2009a,b).

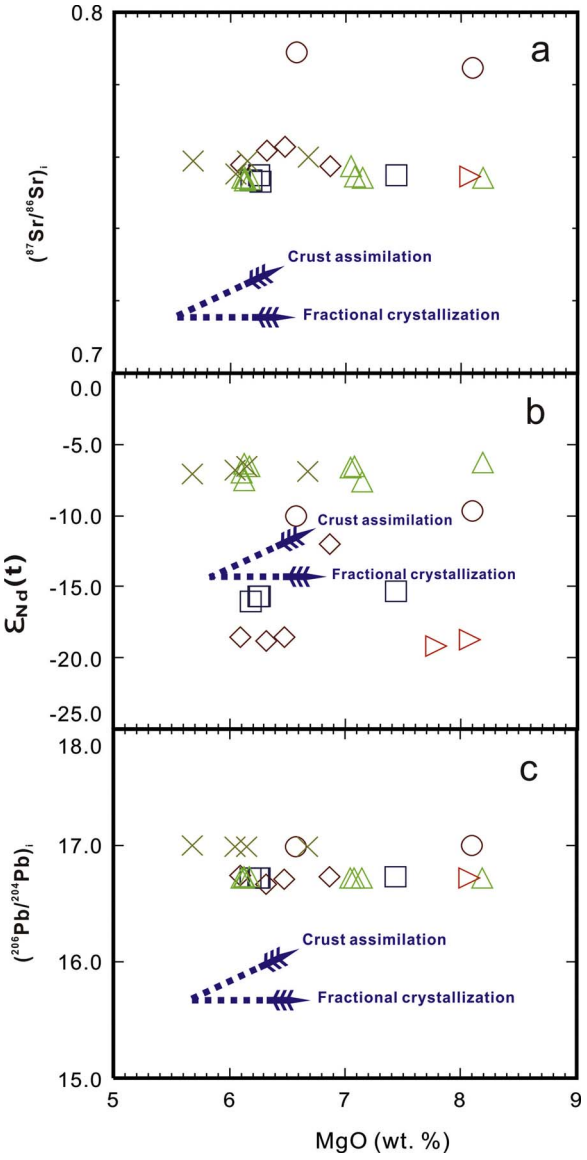

Fig. 12. MgO vs. $(^{87}Sr/^{86}Sr)_i$ (a), ε_{Nd} (t) (b), and $(^{2016}Pb/^{204})_i$ (c) for the mafic dykes in the study areas from the eastern NCC.

7. Thickness of the lithospheric mantle

To discuss the evolution of the lithosphere mantle beneath eastern NCC, the thickness of the Mesozoic mantle must first be constrained. It is generally accepted that the initial lithosphere thickness of the NCC was approximately 80–150 km, and the lithospheric-asthenosphere boundary lay well below this transitional depth (Zhang et al., 2003a,b). If the basaltic rocks have mixed (lithospheric and asthenospheric) isotopic signatures, the lithosphere is between 65 and 80 km thick (Depaolo and Daley, 2000; Zhang et al., 2003a,b). Regression analysis shows a good correlation between the K_2O (x) content of the basaltic rocks and magma source depth (h) ($h \approx 118.69x^{-0.7054}$) in many regions (e.g., Changbaishan, Huinan, Yitong, Shuangliao, and eastern Jilin province) (Fang, 1983; Luo, 1984; Zhang, 1985; Wu, 1985; Yu, 1987). Herein, the deduced process of the above formula between K_2O (x) content and magma source depth (h) is provided as following (Wang et al., 1993). Hypothetically, $h = a\,x^b$, and then the logarithm is taken on both sides of the formula ($\lg h = \lg a + b \lg x$). In addition, lg h is designated as H ($H = \lg h$), lg a is designated as A ($A = \lg a$), and lg x is designated as X ($X = \lg x$), therefore, $\lg h = \lg a + b \lg x$ can be replaced by $H = A + b X$. Based on the least squares principle of linear fitting and necessary conditions for extreme value of multivariate function, the values of A, b, a, and h can be calculated, i.e., $A \approx 2.0744303$, $b \approx -0.705373$, $a \approx 118.69$, and $h \approx 118.69\,x^{-0.7054}$. Adopting this method in the present study, our results indicate that the initial lithosphere thickness was approximately 76.3-79.7 km, and the average thickness is 77.4 km for Longwangmian mafic dykes. For the Weijiazhuang mafic dykes these values are 76.9-77.8 km and 77.3 km, for Mengjiazhuangthe values are 70.8-74.9 km and 74.1 km, for Jiayou 73.6-74.6 km and 73.9 km and for Huangmi these are 61.7-62.9 km 62.3 km respectively. In summary, the initial lithosphere thickness was between 61–80 km, and the average is 74.3 km for the studied dykes. The mafic dykes (Longwangmian and Weijiazhuang, 212 and 199.6 Ma) between late Triassic and early Jurassic show maximum depth (76–80 km), whereas the late Jurassic and early Cretaceous dykes (Mengjiazhuang, Jiayou, Xiahonghe, 136.4 and 123.3 Ma) have medium range (71–75 km). The early Cretaceous dykes from Huangmi (123.5 Ma) show the lowest thickness (61–63 km).

8. Lithospheric thinning and mafic dykes

The NCC remained stable until the early Palaeozoic (460 Ma) (Chi and Lu, 1996). Theoretically, lithospheric foundering would result in lithospheric thinning, and the latter would also lead to voluminous magmatism, and associated mineralization (Kay and Kay, 1993; Liu et al., 2008a,b,c, 2009, 2010), induced by the transformation of lithospheric mantle source (Perry et al., 1988; Dalfy and Depalol, 1992; Wu et al., 2003a,b). The collision between the NCC and Yangtze Craton resulted in crustal thickening and eclogitization of the thickened lower crust. At around ~185 Ma, foundering of eclogites from the lower crust occurred beneath the eastern NCC, triggering asthenospheric upwelling (Liu et al., 2008a,b,c, 2009). In addition, magmatism between 145 Ma and 115 Ma is widespread in the eastern NCC, such as the large-scale

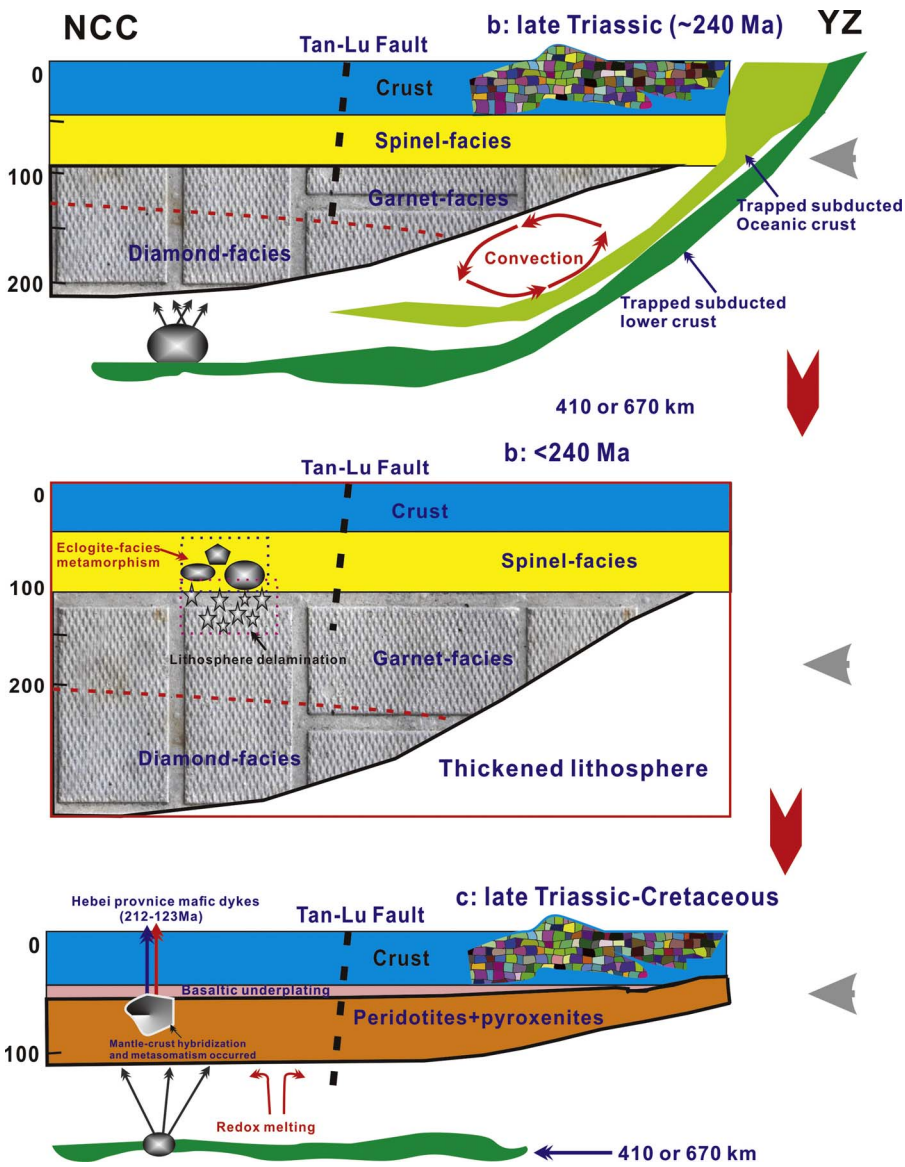

Fig. 13. Schematic model for tectonic evolution in the eastern NCC. (a). ~240 Ma (late Triassic): Dragging of the Yangtze (YZ) lithosphere to a depth of 200 km followed the subduction of the attached oceanic lithosphere (Zhang and Sun, 2002). (b). Less than 240 Ma: The subduction of the YZ craton and its collision with the NCC resulted in thickened lithosphere, followed by delamination of thickened NCC lower crust (Qianxi Group eclogite-facies metamorphism, Jahn and Zhang, 1984) occurred. (c). The intense mantle-crust hybridization and metasomatism (phlogopite, low-Mg amphibole, carbonate-rich magmas or fluids) occurred beneath the study areas. Meanwhile, the lithospheric foundering resulted in lithospheric extension and asthenospheric upwelling. Decompressional melting of the hybridized and metasomatic mantle produce pristine basaltic melts, Subsequently, mafic dykes in the study areas were formed by the fractionation (plagioclase, Ti-bearing oxides and apatite) of basaltic magma.

mafic dykes (Liu, 2004; Liu et al., 2008a,b,c, 2009, 2010), several mafic-intermediate plutons (Guo et al., 2001a,b,c), alkaline complexes (Zhang et al., 2004), and the voluminous Qinshan Formation volcanic rocks (Guo, 1999), together with the formation of extensional basins above a lithosphere that is less than 80 km in thickness (Zhang et al., 2005a,b). It is generally accepted that the extraction of extension-related magma from the lithosphere should lead to further thinning of the lithosphere (Shao and Zhang, 2002; Liu et al., 2006, 2008a,b, 2009, 2010). We thus suggest that 212-123 Ma represents a dominant period of lithospheric thinning beneath the eastern NCC. After 115 Ma, there was no major magmatism prior to the eruption of 85-65 Ma basaltic magmas derived from the asthenospheric mantle. By then, the lithosphere beneath the eastern NCC was thinned to less than 65 km (Yan et al., 2003). We estimate that the lithospheric thickness beneath our study area must be less than 77 km, and thinner (ca. 60 km) in the other areas such as Huangmi and Xiahonghe.

9. Conclusions

Integrated elemental and Sr-Nd-Pb-Hf isotopic studies of the Mesozoic mafic dykes from the eastern NCC allow us to draw the following conclusions.

(1) Mafic dykes from the eastern NCC have EM1-like Sr-Nd-Pb-Hf isotope Signature indicative of derivation from enriched lithosphere mantle.

(2) The EM1-like isotope feature of the mafic dykes suggests a lithospheric Mantle that evolved through line time, and modified considerably by the hybridization of foundered lower crust beneath the eastern NCC.

(3) The depth of magma generation in the mantle sources considerable Variation (61–80 km), suggesting the rapid evolution of lithospheric mantle beneath the eastern NCC. Our results suggest that mantle-crust interaction increased with increasing thickness from Triassic to Cretaceous. The occurrence of widespread mafic dykes investigated in this study suggest an important phase of lithospheric thinning beneath the eastern NCC.

Acknowledgments

We thank Editor Prof. Artemieva and two anonymous referees for constructive comments. This research was financially supported by the National Science Foundation of China (41373028, 41573022).

References

Anderson, D.A., 2006. Speculations on the nature and cause of mantle heterogeneity. Tectonphy. 146, 7–22.

Andersen, T., 2002. Correction of common lead in U-Pb analyses that do not report ^{204}Pb. Chem. Geol. 192, 59–79.

Beier, C., Haase, K.M., Hansteen, T.H., 2006. Magma evolution of the Seta cidades volcano, Sao Miguel, Azores. J. Petrol. 47, 1375–1411.

Chen, B., Jahn, B.M., Arakawa, Y., Zhai, M.G., 2004. Petrogenesis of the Mesozoic intrusive complexes from the southern Taihang orogen, North China Craon: elemental and Sr-Nd-Pb isotopic constraints. Contrib. Mineral. Petrol. 148, 489–501.

Chen, J.F., Yan, J., Xie, Z., Xu, X., Xing, F.M., 2001. Nd and Sr isotopic composition of igneous rocks from the lower Yangtze region in eastern China: Constraints on sources. Phys. Chem. Earth (A) 26, 719–731.

Chi, J.S., Lu, F.X., 1996. The study formation conditons of primary diamond deposits in China. China University of Geosci., Beijing (in Chinese).

Dai, X.L., Peng, S.L., Hu, X.Z., 2010. Adakite in Xiaosigou porphyry cooer-molybdenum deposit, age, geochemical characteristics and geological implications. Miner. Dep. 29, 517–528 (in Chinese with English abstract).

Depaolo, D.J., Daley, E.E., 2000. Neodymium isotopes in basalts of the southwest basin and range and the lithospheric thinning during continental extension. Chem. Geol. 169, 157–185.

Davis, G.A., 2003. The Yanshan belt of north China tectonics, adakitic mafmatism, and crustal evolution. Earth Sci. Frontiers 10, 373–383.

Davis, G., Zheng, Y.D., Wang, C., Darby, B.J., Zhang, C.H., Gehrels, G., 2001. Mesozoic tectonic evolution of the Yangshan fold and thrust belt, withemphasis on Hebei and Liaoning provinces, northern China. In: Hendrix, H.S., Davis, G.A. (Eds.), Paleozoic and Mesozoic Tectonic evolution of Central Asia; From Continental Assembly to Intracontinental Deformation. Geol. Soc. America, Boulder, Colorado, pp. 171–197.

Dalfy, E.E., Depalol, D.J., 1992. Isotopic evidence for lithospheric thinning during extension: southeastern Great Basin. Geol. 20, 104–108.

Dong, Y.P., Santosh, M., 2016. Tectonic architecture and multiple orogeny of the Qinling Orogenic Belt. Central China. Gondwana Res. 29, 1–40.

Dong, S.W., Zhang, Y.Q., Long, C.X., Yang, Z.Y., Ji, Q., Wang, T., Hu, J.M., Chen, X.H., 2007. Jurassic tectonic revolution in China and new interpretation of the Yanshan Movement. Acta Geol. Sinica 81, 1449–1461 (in Chinese with English abstract).

Fang, W.C., 1983. The Cenozoic volcanirc rocks in Jilin province and their tectonic environment. Jilin Geol. 2, 25–33 (in Chinese with English abstract).

Gao, W., Luo, A., Li, L., 2012. Study on mechanism of Mesozoic crust-lithosphere thinning of north China platform. J. Graduates 33, 30–41 (in Chinese with English abstract).

Gao, S., Rudnick, R., Carlson, R.W., McDonough, W.F., Liu, Y.S., 2002. Re-Os evidence for replacement of ancient lithosphere beneath the North China Craton. Earth Planet. Sci. Lett. 198, 307–322.

Gao, S., Rudnick, R.L., Yuan, H.L., Liu, X.M., Liu, Y.S., Xu, W.L., Ling, W.L., Ayers, J., Wang, X.C., Wang, Q.H., 2004. Recycling lower continental crust in the North China Craton. Nature 432, 892–897.

Gao, S., Zhang, B.R., Luo, T.C., Li, Z.J., Xie, Q.L., Gu, X.M., Zhang, H.F., Ouyang, J.P., Wang, D.P., Gao, C.L., 1992. Chemical composition of the continental crust in the Qinling Orogenic Belt and its adjacent North China and Yangtze Cratons. Geochim. Cosmochim. Ccta 6, 3933–3950.

Gao, S., Luo, T.-C., Zhang, B.-R., Zhang, H.-F., Han, Y.-W., Zhang, Z.-D., Hu, Y.-K., 1998a. Chemical et compos ion of the continental crust as revealed by studies in east China. Geochim. Cosmoch. Acta 62, 1959–1975.

Gao, S., Rudnick, R.L., Xu, W.L., Yuan, H.L., Liu, Y.S., Walker, R.J., Puchtel, I., Liu, X.M., Huang, H., Wang, X.R., Yang, J., 2008. Recycling deep cratonic lithosphere and generation of intraplate magmatism in the North China Craton. Earth Planet. Sci. Lett. 270, 41–53.

Gao, S., Zhang, B.-R., Jin, Z.-M., Kern, H., Luo, T.-C., Zhao, Z.-D., 1998b. How mafic is the lower continental crust? Earth Planet. Sci. Lett. 106, 101–117.

Gao, S., Zhang, J.F., Xu, W.L., Liu, Y.S., 2009. The relaship between delamination and destruction of the North China Craton. Chinese Sci. Bull. 54, 1962–1973.

Griffin, W.L., O'Reilly, S.Y., Ryan, C.G., 1992. Composition and thermal structure of the lithosphere beneath south Africa: Siberia and China: Proton microprobe studies. In: Abstract of International Symposium on Genozoic volcanic rocks and deep-seated xenoliths of China and its environs. Beijing. pp. 65–66.

Griffin, W.L., Pearson, N.I., Belousova, E.A., Saeed, A., 2006. Comment: Hf-isotope heterogeneity in zircon 91500. Chem. Geol. 233, 358–363.

Griffin, W.L., Zhang, A.D., O'Reilly, S.Y., Ryan, C.G., 1998. evolution of the lithosphere beneath the Sino-Korean Craton. In: Flower, M.F.J., Chung, S.L., Lo, C.H., Lee, T.Y. (Eds.), In Mantle Dynamics and plate Interactions in East Asia. American Geophy. Union, Geody Ser. 27, pp. 107–126.

Guo, F., 1999. The petrogenesis of Mesozoic volcanic rocks in Shandong province, eastern China and their constraints on the lithosphere thinning process (in Chinese), Ph.D thesis. Inst. of Geotectonic. China. Acad. of Sci., Changsha (in Chinese with English abstract).

Guo, F., Fan, W.M., Wang, Y.J., Lin, G., 2001a. Late Mesozoic mafic intrusive complexes in north China block: constraints on the nature of subcontinental lithospheric mantle. Phys. Chem. Earth (A) 26, 759–771.

Guo, F., Fan, W.M., Wang, Y.J., Lin, G., Li, X.Y., 2001b. Geochemistry of the late Mesozoic mafic magmatism from the eastern North China block: a comparative study. Geotec. et Metall. 25, 1–10 (in Chinese with English abstract).

Guo, Y.Z., Zhao, G.C., Sun, Z.J., Dong, J., 2001c. A petrophysicaa study on genetic-type distribution of intrusive rocks and marginal ore-forming frocess in Hebei province. Geophy. Geoch. Expl. 25, 372–378 (in Chinese with English abstract).

Guo, F., Guo, J.T., Wang, Y.C., Fan, W.M., Li, C.W., Zhao, Liang, Li, H.X., Li, J.Y., 2013. Formation of mafic magmas through lower crustal AFC processes-An example from the Jinan gabbroic intrusion in the North China Block. Lithos 179, 157–174.

Guo, F., Fan, W.M., Wang, Y.J., Zhang, M., 2004. Origin of early Cretaceous calc-alkaline lamprophyres from the Sulu orogen in eastern China: implications for enrichment processes beneath continental collisional belt. Lithos 78, 291–305.

Guo, J.H., Sun, M., Chen, F.K., Zhai, M.G., 2005. Sm-Nd and SHRIMP U-Pb zircon geochronology of high-pressure granulites in the Sanggan area, North China Craton: timing of Palaeoproterozoic continental collision. J. Asian Earth Sci. 24, 629–642.

Hart, S.R., 1984. A large-scale isotope anomaly in the southern Hemisphere mantle. Nature 309, 753–757.

Hartrnann, G.W., Wedepohl, K.H., 1990. Metasomatically latered peridotite xenoliths from the Hessian depression (NW Germany). Geochim. Cosmochim. Acta 54, 71–86.

Herzberg, C., Asimow, P.D., Arndt, N., Niu, Y., Lesher, C.M., Fitton, J.G., Cheadle, M.J., Saunders, A.D., 2007. Temperatures in ambient mantle and plumes: constraints from basalts, picrites, and komatiites. Geochem. Geophy. Geosys. 8, Q02006. http://dx.doi.org/10.1029/2006GC001390.

Hirajima, T., Ishiwatari, A., Cong, B., Zhang, B., Zhang, R., Banno, S., Nozaka, T., 1990. Coesite from Mengzhong eclogite at Donghai county, northern Jiangsu provnice, China. Mineral. Ma. 54, 579–583.

Hong, D.W., Wang, T., Tong, Y., Wang, X.X., 2003. Mesozoic granitoids from North China Block and Qinling-Dabie-Sulu orogenic belt and their deep dynamic process. Earth Sci. Frontiers 10, 231–256 (in Chinese with English abstract).

Jahn, B.M., Wu, F.Y., Lo, C.H., Tsai, C.H., 1999. Crust-mantle interaction induced by deep subduction of the continental crust: geochemical and Sr-Nd isotopic evidence from post-collisional mafic-ultramafic intrusions of the northern Dabie complex central China. Chem. Geol. 157, 119–146.

Jahn, B.M., Zhang, Z.Q., et al., 1984. Radiometric ages (Rb-Sr, Sm-Nd, U-Pb) and REE geochemistry of Arcehan granulite gneisses from eastern Hebei province, China. In: Kroner, A. (Ed.), Archean geochemistry. Springer-Verlag, Beijing, pp. 204–234.

Jochum, K.P., McDonough, W.F., Palme, H., Spettel, B., 1989. Compositionalconstraints on the continental lithospheric mantle from trace elements in spinel peridotite xenoliths. Nature 340, 548–550.

JÖrg, A., Pfänder, J.A., Münker, C., Stracke, A., Mezger, K., 2007. Nb/Ta and Zr/Hf in ocean island basalts-Implications for crust-mantle differentiation and the fate of Niobium. Earth Planet. Sci. Lett. 254, 158–172.

Jull, M., Kelemen, P.B., 2001. On the conditions for lower crust convective instability. J. Geophy. Res. 106, 6423–6446.

Kato, T., Enami, A., Zhai, M., 1997. Ultrahigh-pressure marble and eclogite in the Su-Lu ultrahigh-pressure terrane, eastern China. J. Metamor. Geol. 15, 169–182.

Kay, R.W., Kay, S.M., 1991. Creation and destruction of lower continental crust. Geol. Rundsch 80, 259–278.

Kogiso, T., Hirschmann, M.M., Frost, D.J., 2003. High-pressure partial melting of garnet dyroxenite: possible mafic lithologies in the source of ocean island basalts. Earth Planet. Sci. Lett. 216, 603–617.

Le Maitre, E.W., Bateman, P., Dubek, A., Keller, J., Lameyre, J., Le Bas, M.J., Sabine, P.A., Schimid, R., Sorensen, H., 1989. *A classification of Igneous rocks and Glossary of Terms*: Recommendations of the Inter-national Univon of Geological Sciences Sbudommission on the Systematics of Igneous rocks. Blackwell Oxford.

Le Maitre, R.W., 2002. Igneous rocks: A classification and glossary of Terms, 2nd: *Cambridge University. Pre.* Cambridge 236.

Levander, A., Niu, F., Lee, C.T.A., Cheng, X., 2006. Imaging the contiental lithosphere. Tectonphy. 416, 167–185.

Li, C.W., Guo, F., Li, X.Y., 2004. Geochemistry of late Mesozoic mafic volcanic rocks in Lishui basin and their tectonic implications. Geoch. 33, 361–371 (in Chinese with English abstract).

Li, Q., Santosh, M., Li, S.R., Zhang, J.Q., 2015. Petrology, geochemistry and zircon U-Pb and Lu-Hf isotopes of the Cretaceous dykes in the central North China Craton: implications for magma genesis and gold metallogny. Ore Geol. Rev. 67, 57–77.

Li, Q.Z., 2007. Pb-Sr-Nd isotopic characteristics of the early Cretaceous mafic rocks from eastern China: the contribution of the lower crust to the mantle source. PhD thesis of University of Sci. Tec. 1–161 (in Chinese with English abstract).

Li, S.G., Huang, F., Li, H., 2002. Post-collisional delamination of the lithosphere beneath Dabie-Sulu orogenic belt. Chinese Sci. Bull. 46, 1487–1490.

Li, S.G., Xiao, Y.L., Liou, D.L., Chen, Y.Z., Ge, N.J., Zhang, Z.Q., Sun, S.S., Cong, B.L., Zhang, R.Y., Har, S.R., Wang, S.S., 1993. Collision of the North China and Yangtze Blocks and formation of coesite-bearing eclogites-Timing and processes. Chem. Geol. 109, 89–111.

Li, S.R., Santosh, M., 2017. Geodynamics of heterogeneous gold mineralization in the North China Craton and its relationship to lithospheric destruction. Gondwana Research 50, 267–292.

Li, S.Z., Zhao, G.C., Sun, M., Han, Z.Z., Zhao, G.T., Hao, D.F., 2006. Are the South and North Liaohe Groups of the North China Craton different exotic terranes? Nd isotope constraints. Gondwana Res 9, 198–208.

Li, S.Z., Zhao, G.C., 2007. SHRIMP U-Pb zircon geochronology of the Liaoji granitoids: constraints on the evolution of the Paleoproterozoic Jiao-Liao-Ji belt in the Eastern Block of the North China Craton. Precambian. Res. 158, 1–16.

Li, X.P., Yang, Z.Y., Zhao, G.C., Grapes, R., Guo, J.H., 2011. Geochronology fkhondalite-series rocks of the Jining Complex: confirmation of epositional age andtectonometamorphic evolution of the North China craton. Int. Geol. Rev. 53, 1194–1211.

Liu, D.Y., Nutman, A.P., Compston, W., Wu, J.S., Shen, Q.H., 1992. Remnants of 3.8 Ga crust in the Chinese part of the Sino-Korean craton. Geol. 20, 339–342.

Liu, J.L., Ji, M., Xia, H.R., Liu, Z.H., Zhou, Y.S., Yu, X.Q., Zhang, H.Y., Cheng, S.H., 2009a. Crustal-mantle detachment of the North China Craton in late Mesozoic: Rheological constraints. Acta Petrol. Sinica 25, 1819–1829 (in Chinese with English abstract).

Liu, S., Hu, R.Z., Gao, S., Feng, C.X., Yu, B.B., Feng, G.Y., Qi, Y.Q., Wang, T., Coulson, I.M., 2009b. Petrogenesis of Late Mesozoic mafic dykes in the Jiaodong Peninsula,

eastern North China Craton and implications for the foundering of lower crust. Lithos 113, 621–639.
Liu, S., 2004. The Mesozoic mgmatism and crustal extension in Shandong Province, China–additional discussing the relationship between lamprophyres and gold mineralization. Ph. D. thesis. Inst. of Geochm. Chin. Acad. Of Sci., Guiyang (in Chinese).
Liu, S., Feng, C.X., Jahn, B.M., Hu, R.Z., Gao, S., Feng, G.Y., Lai, S.C., Yang, Y.H., Qi, Y.Q., Coulson, I.M., 2013. Geochemical, Sr-Nd isotopic, and zircon U-Pb geochronological constraints on the petrogenesis of Late Paleoproterozoic mafic dykes within the northern North China Craton, Shanxi Province. China. Precambrian Research 206, 182–192.
Liu, S., Hu, R.Z., Feng, G.Y., Yang, Y.H., Feng, C.X., Qi, Y.Q., Wang, T., 2010. Distribution and significance of the mafic dyke swarms since Mesozoic in North China Craton. Geol. Bull. China 29, 259–267 (in Chinese with English abstract).
Liu, S., Hu, R.Z., Gao, S., Feng, C.X., Qi, L., Zhong, H., Xiao, T., Qi, Y.Q., Wang, T., Coulson, I.M., 2008a. Zircon U-Pb geochronology and major trace elemental and Sr-Nd-Pb isotopic geochemistry of mafic dykes in western Shandong Province, east China: constrains on their petrogenesis and geodynamic significance. Chem. Geol. 255, 329–345.
Liu, S., Hu, R.Z., Gao, S., Feng, C.X., Qi, Y.Q., Wang, T., Feng, G.Y., Coulson, I.M., 2008b. U-Pb zircon age, geochemical and Sr-Nd-Pb-Hf isotopic constraints on age and origin of alkaline intrusions and associated mafic dikes from Sulu orogenic belt, eastern China. Lithos 106, 365–379.
Liu, J.L., Davis, G.A., Ji, M., Guan, H.M., Bai, X.D., 2008c. Crustal detachment and destruction of the North China Craton: constraints from Late Mesozoic extensional structures. Earth Sci. Front. 15, 72–81 (in Chinese with English abstract).
Liu, Y.S., Gao, S., Lee, C.-T., 2005. Melt-peridotite interactions: Links between garnet pyroxenite and high-$Mg^{\#}$ signature of continental crust. Earth Planet. Sci. Lett. 234, 39–57.
Lu, F.X., Zheng, J.P., Li, W.P., Chen, M.H., Chen, Z.M., 2000. The main evolution pattern of Phanerozoic mantle in the eastern China: the Mushroom cloud model. Earth Sci. Front. 7, 97–107 (in Chinese with English abstract).
Lu, F.X., Zheng, J.P., Shao, J.A., Zhang, R.S., Chen, M.H., Yu, C.M., 2006. Asthenospheric upwelling and lithospheric thinning in late Cretaceous Cenozoic in eastern North China. Earth Sci. Front. 13, 86–92 (in Chinese with English abstract).
Ludwig, K.R., 2003. User's manual for Isoplot/Ex. Version 3.00. A Geochronological Toolkit for Microsoft Excel, 4. Berkeley Geochronology Center Special Publication, pp. 1–70.
Luo, Z.H., 1984. Dayishan alkali basalt, Huinan county, Jilin province and its origin. Earth Sci. 24, 73-80 (in Chinese with English abstract).Ma, G.X., 1997. Geological characteristics and metallogenic model of copper deposit at Muji village of Laiyuan county, Hebei province. J. Geol. & Min. Res. 12, 52–66 (in Chinese with English abstract).
Meng, Q.R., Zhang, G.W., 2000. Geologic framework and tectonic evolution of the Qinling orogen, central China. Tectonophysics 323, 183–196.
Menzies, M.A., Fan, W.M., Zhang, M., 1993. Paleozoic and Cenozoic lithoprobes and the loss of > 120 km of Achaean lithosphere, Sino-Korean craton, China. In: Prichard, H.M., Alabaster, T., Harris, N.B.W., Neary, C.R. (Eds.), Magmatic Processes and Plate Tectonics. Geol. Soc. Special Pub. 76, pp. 71–78.
Menzies, M.A., Xu, Y.G., 1998. Geodynamics of the North China Craton. In: Flower, M.F.J., S.L.Chung, C.H., Lo, T.Y. (Eds.), Mantle Dynamics and Plate Interactions in east Asia. American Geophy. Union, Geody Ser. 27, pp. 155–165.
Menzies, M.A., Xu, Y.G., Zhang, H.F., 2007. Intergration of geology: geophysics and geochemistry: A key to understanding the North China Craton. Lithos 96, 1–21.
Middlemost, E.A.K., 1994. Naming materials in the magma/igneous rock system. Earth-Sci. Rev. 74, 193–227.
Mu, B.L., Shao, J.A., Chu, Z.Y., 2001. Sm-Nd age and Sr, Nd, Pb isotopic characteristics of the patassic alkaline ultra-mafic syenitic complex, Fanshan, Hebei province. Acta Petrol. Sin. 17, 358–365 (in Chinese with English abstract).
Mu, B.L., Yan, G.H., 1992. Geochemistry of Triassic alkaline or subalkaline igneous complexes in the Yanliao area and their significane. Acta Geol.Sinica. 66, 108–121 (in Chinese with English abstract).
Nie, F.J., Jiang, S.H., Bai, D.M., Hou, W.R., Liu, Y.G., 2010. Types and temporal-spatial distribution of metallic deposits in southern Mongolia and its neighboring areas. Acta Geosci. Sinica 31, 267–288 (in Chinese with English abstract).
Niu, Y.L., 2005. Generation and evolution of basaltic magmas: some basic concepts and a new view on the origin of Mesozoic-Cenozoic basaltic volcanism in eastern China. Geol. J. China University 11, 9–46.
O'Reilly, S.Y., Griffin, W.L., Poudjom Djomani, Y.H., Morgan, P., 2001. Are lithospheres forever? Tracking chages in sub-continental lithospheric mantle through time. GSA Today 11, 4–10.
Perry, F.V., Baldridge, S., Depaolo, D.J., 1988. Chemical andisotopic evidence for lithospheric thinning beneath the Rio Grande rift. Nature 332, 432–434.
Poudjom Djomani, Y.H., O'Reilly, S.Y., Griffin, W.L., Morgan, P., 2001. The density structure of sub-continental lithosphere through time. Earth Planet. Sci. Lett. 184, 605–621.
Qi, L., Hu, J., Grégoire, D.C., 2000. Determination of trace elements in granites by inductively coupled plasma mass spectrometry. Talanta 51, 507–513.
Rapp, R.P., Shimizu, N., Norman, M.D., 2003. Growth of early continental crust by partial melting of eclogite. Nature 425, 605–609.
Rgional Geology of Gansu Province, 1989. Geological Publishing House.
Regional Geology of Hebei Province, Beijing, T ianjin, 1982. Geological Publishing House.
Regional Geology of Henan Province, 1989. Geological Publishing House.
Regional Geology of Liaoning Province, 1989. Geological Publishing House.
Regional Geology of Shanxi Province, 1989. Geological Publishing House.
Regional Geology of Shaanxi Province, 1989. Geological Publishing House.
Regional Geology of Inner Mongolia Autonomous Region, 1991. Geological Publishing House.
Robinson, P.T., Zhou, M.G., Hu, X.F., Reynolds, P., Bai, W.J., Yang, J.S., 1999. Geochemical constraints on the origin of the Hegenshan ophiolite, Inner Mongolia, China. J. Asian Earth Sci. 17, 423–442.
Roden, M., Murthy, V.R., 1985. Mantle metasomatism. Ann. Rev. Earth Planrt. Sci. Lett. 13, 269–296.
Rudnick, R.L., Barth, M., Horn, I., McDonough, W.F., 2000. Rutile-bearing refractory eclogites: missing link between continents and depleted mantle. Science 287, 278–281.
Rudnick, R.L., McDonouth, W.F., Chapell, B.W., 1993. Carbonatite metasomatism in the northern Tnzanian mantle: petrographic and geochemical charateristics. Earth Planet. Sci. Lett. 114, 463–475.
Santosh, M., 2010. Assembling North China Craton within the Columbia supercontinent: The role of double-sided subduction. Precambrian Res. 178, 149–167.
Santosh, M., Liu, S.J., Tsunogae, T., Li, J.H., 2012. Paleoproterozoic ultrahigh-temperature granulites in the North China Craton: Implications for tectonic models on extreme crustal metamorphism. Precambrian Res. 222–223, 77–106.
Shao, J.A., Zhang, L.Q., 2002. Mesozoic dyke swarms in the north of north China. Acta Petrol. Sinica 18, 312–318 (in Chinese with English abstract).
Sobolev, A.V., Hofmann, A.W., Sobolev, S.V., Nikogosian, I.K., 2005. An olivine-free mantle source of Hawaiian shield basalts. Nature 434, 590–597.
Sun, S.S., McDonough, W.F., 1989. Chemical and isotopic systematics of oceanic basalts: Implications for mantle composition and processes. In: Saunders, A.D., Norry, M.J. (Eds.), Magmatism in the Ocean basins. Geol. Society Spec. Pub., London, pp. 313–345.
Tam, P.Y., Zhao, G.C., Sun, M., Li, S.Z., Wu, M.L., Yin, C.Q., 2012b. Petrology and metamorphic P-T path of high-pressure mafic granulites from the Jiaobei massif in the Jiao-Liao-Ji Belt, North China Craton. Lithos 155, 94–109.
Tam, P.Y., Zhao, G.C., Zhou, X.W., Sun, M., Li, S.Z., Yin, C.Q., Wu, M.L., He, Y.H., 2012a. Metamorphic P-T path and implications of high-pressure pelitic granulites from the Jiaobei massif in the Jiao-Liao-Ji Belt. North China Craton. Gondwana Res. 22, 104–117.
Tang, Y.J., Zhang, H.F., Ying, J.F., Zhang, J., Liu, X.M., 2008. Refertilization of ancient lithospheric mantle beneath the central North China Craton; Evidence from petrology and geochemistry of peridotite xenoliths. Lithos 101, 435–452.
Tong, J.Q., 2016. Geological characteristics, metallogenic conditions and prospecting direction of Shihu gold deposit in Lingshou country, Hebei province. Master's thesis of Jilin University 1–57 (in Chinese with English abstract).
Wang, F., Li, X.P., Chu, H., Zhao, G.C., 2011. Petrology and metamorphism of khondalites from Jining Complex in the North China Craton. Int. Geol. Rev. 53, 212–229.
Wang, F.Y., Gao, S., Niu, B.G., Zhang, H., 2007a. Geochemistry of Dabeigou basalt in Chende basin, Hebei province and constraints on lithospheric mantle tinning of North China Craton. Eartth Sci. Front. 14, 98–108 (in Chinese with English abstract).
Wang, T., Zheng, Y.D., Zhang, J.J., Wang, X.S., Zeng, L.S., Tong, Y., 2007b. Some problems in the study of Mesozoic extensional structure in the North China Craton and its significance for the study of lithospheric thinning. Geol. Bull. China 26, 1154–1166 (in Chinese with English abstract).
Wang, X.K., Zhao, L., Sui, W.G., Xu, M.X., 1993. Correlation analysis on K_2O content with magma genetic depth and diagenetic age for Cenozoic alkali basalts in eastern Jilin province. Journal of Changchun University of Earth Sciences 23, 416–422 (in Chinese with English abstract).
Wang, Y.J., Fan, W.M., Zhang, H.F., Peng, T.P., 2006. Early Cretaceous gabbroic rocks from the Taihang Mountains: implications for a paleosubduction-related lithospheric mantle beneath the central North China Craton. Lithos 86, 281–302.
Wen, C.G., Zhen, Y.Q., Diao, Q., Chen, Z., Song, T., Zhang, Y.J., Qiao, H., 2016. Lithosphere destruction and mantle plume genesis of eastern North China Craton. Contib. Geol. Mineral Resources. Res. 31, 1–17 (in Chinese with English abstract).
Wilde, S.A., Zhao, G.C., Sun, M., 2002. Development of the North China craton during the Late Archaean and its final amalgamation at 1.8 Ga: some speculation on its position within a global Palaeoproterozoic Supercontinent. Gondwana Res. 5, 85–94.
Wilde, S.A., Zhou, X.H., Nemchin, A.A., Sun, M., 2003. Mesozoic crust mantle interaction beneath the North China Craton: a consequence of the dispersal of Gondwanaland and accretion of Asia. Geol. 31, 817–820.
Wu, F.Y., Ge, W.C., Sun, D.Y., Guo, C.L., 2003a. Discussions on the lithopheric thinning in eastern China. Earth Sci. Front. 10, 51–60 (in Chinese with English abstract).
Wu, F.Y., Walker, R.J., Ren, X.W., Sun, D.Y., Zhou, X.H., 2003b. Osmium isotopic constraints on the age of lithospheric mantle beneath northeastern China. Chem. Geol. 197, 107–129.
Wu, F.Y., Lin, J.Q., Wilde, S.A., Zhang, X.O., Yang, J.H., 2005. Nature and significance of the early Cretaceous giant igneous event in eastern China. Earth Planet. Sci. Lett. 233, 103–119.
Wu, F.Y., Walker, R.J., Yang, Y.H., Yuan, H.L., Yang, H.H., 2006a. The chemical-temporal evolution of lithospheric mantle underlying the North China Craton. Geochim. Cosmochim. Acta 70, 5013–5034.
Wu, F.Y., Yang, Y.H., Xie, L.W., Yang, I.H., Xu, P., 2006b. Hf isotopic compositions of the standard zircons and baddeleyites used in U-Pb geochronology. Chem. Geol. 234, 105–126.
Wu, F.Y., Sun, D.Y., Zhang, G.L., Ren, X.W., 2000. Deep geodynamics of Yanshain movement. Geol. J. China Universe. 6, 379–388 (in Chinese with English abstract).
Wu, F.Y., Xu, Y.G., Gao, S., Zheng, J.P., 2008. Lithospheric thinning and destruction of the North China Craton. Acta Petrol. Sinica 24, 1145–1174 (in Chinese with English abstract).
Wu, L.Y., 1985. The study on the upper mantle xenoliths from Cenozoic basalts in Yitong, Jilin province. Jilin province 1-14 (in Chinese).
Xia, X.P., Sun, M., Zhao, G.C., Wu, F.Y., Xu, P., Zhang, J.S., 2008. Paleoproterozoic crustal growth events in the Western Block of the North China Craton: Evidence from detrital

zircon Hf and whole rock Sr-Nd isotopes of the khondalites in the Jining Complex. American J. Sci. 308, 304–327.
Xiao, C., 2016. Chronology, geochemistry and petrogenesis of Mesozoic volcanic rocks from Qinglong area of Hebei and Jianchang area of Liaoning. Master's thesis of Jilin University 1–49 (in Chinese with English abstract).
Xie, Z., Li, Q.Z., Gao, T.S., 2006. Comment on petrogenesis of post-orogenic syenites in the Sulu orogenic belt, east China: geochronological, geochemical and Nd-Sr isotopic evidence by Yang et al. Chem. Geol. 235, 191–194.
Xiong, X.L., Liu, X.C., Zhu, Z.M., Liu, Y., Xiao, W.S., Song, M.S., Zhang, S., Wu, J.H., 2011. The adakitic rocks and destruction of the North China Craton: evidence from experimental petrology and geochemistry. Sci. China 5, 654–667 (in Chinese with English abstract).
Xu, W.L., Hergt, J.M., Gao, S., Pei, F.P., Wang, W., Yang, D.B., 2008. Interaction of adakitic melt-peridotite: implications for the high-Mg# signature of Mesozoic adakitic rocks in the eastern North China Craton. Earth Planet. Sci. Lett. 265, 123–137.
Xu, W.L., Wang, Q.H., Wang, D.Y., Pei, F.P., Gao, S., 2004. Processes and mechanism of Mesozoic lithospheric thinning in eastern North China Craton:Evidence from Mesozoic igneous rocks and deep-seated xenoliths. Earth Sci. Front. 11, 309–317 (in Chinese with English abstract).
Xu, W.L., Yang, C.H., Yang, D.B., Pei, F.P., Wang, Q.H., Ji, W.Q., 2006. Mesozoic high-Mg idorites in eastern North China Craton: constraints on the mechanism of lithospheric thinning. Earth Sci. Frontiers 13, 120–129 (in Chinese with English abstract).
Xu, Y.G., 2001. Thermo-tectonic destruction of the Archean lithospheric keel beneath the Sino-Korean Craton in China: Evidence, timing and mechanism. Phys. Chem. Earth (A) 26, 747–757.
Xu, Y.Y., Xu, H.C., Shen, Z., Li, X.H., Zhao, H.P., Zhang, L.G., Lyu, Y.Q., 2016. Geochemical characteritics of magmatic rocks with differnet ages in Guyuan area, Hebei province. Geol. Sur. Res. 39, 95–103 (in Chinese with English abstract).
Yan, G.H., Cai, J.H., Ren, K.X., He, G.Q., Mu, B.L., Xu, B.L., Li, F.T., Yang, B., 2007. Intraplate extensional magmatism of North China Craton and break-up of three supercontinents and their deep dynamics. Geol. J. China Universities 13, 161–174 (in Chinese with English abstract).
Yan, J., Chen, J.F., Yu, G., Qian, H., Zhou, T.X., 2003. Pb isotopic characteristics of late Mesozoic mafic rocks from the lower Yangtze Region: evidence for enriched mantle. J. China University Geosci. 9, 195–206 (in Chinese with English abstract).
Yang, J., 1991. The geochemical features and their genesis of lamprophyres in Laiyuan-Fuping area, Hebei province. China. China University Geosci. 5, 330–337 (in Chinese with English abstract).
Yang, Q.Y., Santosh, M., 2015. Paleoproterozoic arc magmatism in the North China Craton: No Siderian global plate tectonic shutdown. Gondwana Research 28, 82–105.
Yang, Q.Y., Santosh, M., 2017. The building of an Archean microcontinent: Evidence from the North China Craton. Gondwana Research 50, 3–37. http://dx.doi.org/10.1016/j.gr.2017.01.003.
Yang, Q.Y., Santosh, M., Collins A. s. Teng, X.M., 2016. Micro-block amalgamation in the North China Craton: Evidence from Neoarchaean magmatic suite in the western margin of the Jiaoliao Block. Gondwana Research 31, 96–123.
Yang, J.H., Sun, J.F., Chen, F.K., Wilde, S.A., Wu, F.Y., 2007a. Sources and petrogenesis of Late Triassic dolerite dikes in the Liaodong Peninsula: Implications for post-collisional lithosphere thinning of Eastern North China Craton. Journal of Petrology 48, 1973–1997.
Yang, J.H., Wu, F.Y., Wilde, S.A., Liu, X.M., 2007b. Petrogenesis of Late Triassic granitoids and their enclaves with implications for post-collisional lithospheric thinning of the Liaodong Peninsula, North China Craton. Chemical Geology 242, 155–175.
Yang, J.H., Wu, F.Y., Wilde, S.A., 2008. Mesozoic decratonization of the North China block. Geol. 36, 467–470.
Yang, Y.H., Liu, S., Hu, R.Z., Feng, C.X., Qi, Y.Q., Yang, C.G., Tang, L., 2013. Geochemical features and petrogenesis of Houcheng mafic dyke in Hebei: evidence from major and trace elements. Geol. Bull. China 32, 607–616 (in Chinese with English abstract).
Yaxley, G.M., 2000. Experimental study of the phase and melting relations of homogeneous basalt + peridotite mixtures and implications for the petrogenesis of flood basalts. Contrib. Mineral. Petrol. 139, 326–338.
Yin, C.Q., Zhao, G.C., Guo, J.H., Sun, M., Zhou, X.W., Zhang, J., Xia, X.P., Liu, C.H., 2011. U-Pb and Hf isotopic study of zircons of the Helanshan Complex: constraints on the evolution of the Khondalite Belt in the Western Block of the North China Craton. Lithos 122, 25–38.
Yin, C.Q., Zhao, G.C., Sun, M., Xia, X.P., Wei, C.J., Zhou, X.W., Leung, W.H., 2009. LA-ICP-MS U-Pb zircon ages of the Qianlishan Complex: constraints on the evolution of the Khondalite Belt in the Western Block of the North China Craton. Precambrian Res. 174, 78–94.
Ying, J.F., Zhang, H.F., Sun, M., Tang, Y.J., Zhou, X.H., Liu, X.M., 2007. Petrology and geochemistry of zijinshan alkaline intrusive complex in Shanxi province, western North China Craton: implications for magma mixing of different sources in an extensional regime. Lithos 98, 45–66.
Yu, Y., 1987. Petrology and petrogenesis of the Cenozoic basaltic rocks from Mt. Qixingshan, Jilin province. Acta Petrol. Sinica 3, 55–63 (in Chinese with English abstract).
Yuan, H.L., Gao, S., Liu, X.M., Li, H.M., Gunther, D., Wu, F.Y., 2004. Accurate U-Pb age and trace element determinations of zircon by laser ablation-inductively coupled plasma mass spectrometry. Geostandards Newsletter 28, 353–370.
Yuan, X.C., 1996. The lithosphere and mushroom cloud structure modal in Qinling Mt. Sci. China (D) 26, 209–215 (in Chinese).
Yuan, X.C., 2007. Mushroom structure of the lithospheric mantle and its genesis at depth: revisited. Geol. China 34, 737–758 (in Chinese with English abstract).
Zhai, M.G., 2010. Tectonic evolution and metallogenesis of North China Craton. Mineral Deposits 29, 24–36 (in Chinese with English abstract).
Zhai, M.G., Bian, A.G., 2000. Supercontinent flatten in late Neoarchean and the cracking during Paleoproterozoic and Mesoproterozoic of the NCC. Sci. China 30, 129–137.
Zhai, M.G., Meng, Q.R., Liu, J.M., Hou, Q.L., Hu, S.B., Liu, Z., Zhang, H.F., Liu, W., Shao, J.A., Zhu, R.X., 2004. Geological features of Mesozoic tectonic regime inversion in eastern North China and implication for geodynamics. Earth Sci. Front. 11, 285–297 (in Chinese with English abstract).
Zhai, M.G., Santosh, M., 2011. The early Precambrian odyssey of the North China Craton. A synoptic overview. Gondwana Res. 20, 6–25.
Zhang, B.M., Ma, G.X., Bi, F.K., Zhao, G.L., 1996. Magmatism associated metallogenic series and metallogenic model of the main metallogenic zone in Hebei. J. Geol. & Min. Res. North China 11, 51–60 (in Chinese with English abstract).
Zhang, B.Z., 1985. The investigation report of the Yintong volcanic group. Jilin province (in Chinese with English abstract).
Zhang, H.F., 2009. Peridotite-melt interaction: the major factor for the destruction of the cratonic lithospheric mantle. China Sci. Bull. 54, 2008–2026 (in Chinese).
Zhang, H.F., Nakamura, E., Sun, M., Kobayashi, K., Zhang, J., Ying, J.F., Tang, Y.J., Niu, L.F., 2007. Transformation of sub-continental lithospheric mantle through peridotite-melt reaction: evidence from a highly fertile mantle xenolith from the North China Craton. Int. Geol. Rev. 49, 658–679.
Zhang, H.F., Sun, M., Lu, F.X., Zhou, X.H., Zhou, M., Liu, Y.S., Zhang, G.H., 2001. Geochemical significance of a garnet lherzolite from the Dahongshan kimberlite, Yangtze Craton, southern China. Geochem. J. 35, 315–331.
Zhang, H.F., Sun, M., Zhou, M.F., Fan, W.M., Zhou, X.H., Zhai, M.G., 2004. Highly heterogeneous late Mesozoic lithospheric mantle beneath the North China Craton: evidence from Sr-Nd-Pb isotopic systematics of mafic igneous rocks. Geol. Mag. 141, 55–62.
Zhang, H.F., Sun, M., Zhou, X.H., Fan, W.M., Zhai, M.G., Yin, J.F., 2002. Mesozoic lithosphere destruction beneath the North China Craton: evidence from major-, trace-element and Sr-Nd-Pb isotope studies of Fangcheng basalts. Contrib. Mineral. Petrol. 144, 241–253.
Zhang, H.F., Sun, M., Zhou, X.H., Ying, J.F., 2005a. Geochemical constraints on the origin of Mesozoic alkaline intrusive complexes from the North China Craton and tectonic implicaitons. Lithos 81, 297–317.
Zhang, Q., Li, C.D., Wang, Y., Wang, Y.L., Jin, W.J., Han, S., 2005b. Mesozoic high-Sr and Low-Yb granitoids and low-Sr and High-Yb granitoids in eastern China: comparison and geological implications. Acta Petrol. Sinica 21, 1527–1537 (in Chinese with English abstract).
Zhang, H.F., Sun, M., Zhou, X.H., Zhou, M.F., Fang, W.M., Zheng, J.P., 2003a. Secular evolution of the lithosphere beneath the eastern North China Craton: Evidence from Mesozoic basalts and high-Mg andesites. Geochim. Cosmochim. Acta 67, 4373–4387.
Zhang, Q., Wang, Y., Liu, H.T., Wang, Y.L., Li, Z.T., 2003b. On the space-time distribution and geodynaic environments of adakites in China annex: controversies over differing openions for adakites in China. Earth Sci. Frontiers 10, 385–400 (in Chinese with English abstract).
Zhang, R.Y., Hirajima, T., Banno, S., Cong, B., Liou, J.G., 1995. Petrology of ultrahigh-pressure metamorphic rocks in southern Sulu region, eastern China. J. Metamor. Geol. 13, 659–675.
Zhao, G.C., 2009. Metamorphic evolution of major tectonic units in the basement ofthe North China Craton: key issues and discussion. Acta Petrol. Sinica 25, 1772–1792 (in Chinese with English abstract).
Zhao, G.C., Gawood, P.A., Li, S.Z., Wilde, S.A., Sun, M., Zhang, J., He, Y.H., Yin, C.Q., 2012. Amalgamation of the North China Craton: key issue and discussion. Precambrian Res. 222 (-223), 55–76.
Zhao, G.C., Sun, M., Wilde, S.A., Li, S.Z., 2005. Late Archaean to Palaeoproterozoic evolution of the North China craton: key issues revisited. Precambrian Res. 136, 177–202.
Zhao, G.C., Wilde, S.A., Cawood, P.A., Sun, M., 2001. Archean blocks and their boundaries in the North China Craton: lithological geochemical, structural and P-T path constraints and tectonic evolution. Precambrian Res. 107, 45–73.
Zhao, G.C., Wilde, S.A., Cawood, P.A., Sun, M., 2002. SHRIMP U-Pb zircon ages of the Fuping complexes: implications for late Archean to Paleoproterozoic accretion and assembly of the North China Craton. Am. J. Sci. 302, 191–226.
Zhao, G.C., Wilde, S.A., Guo, J.H., Gawood, P.A., Sun, M., Li, X.P., 2010. Single zircon grains record two paleoproterozoic collisional events in the North China Craton. Precam. Res. 177, 266–276.
Zhao, G.C., Zhai, M.G., 2013. Lithotectonic elements of Precambrian basement in the North China Craton: review and tectonic implications. Gondwana Res. 23, 1207–1240.
Zhao, Z.F., Zheng, Y.F., Wei, C.S., Wu, Y.B., 2004. Zircon isotope evidence for recycling of subducted continental crust in post-collisional granitoids from the Dabie terrane in China. Geophy. Res. Lett. 31 2004GL021061.
Zheng, J.P., 1999. Mesozoic-Cenozoic mantle replacement and lithospheric thinning, east China (in Chinese with English abstract). Univer. Geosci. Press, China.
Zheng, J.P., Griffin, W.L., O'Reilly, S.Y., 2006. Mineral chemistry of garnet peridotites from Paleozoic: Mesozoic and Cenozoic lithosphere: constraints on mantle evolution beneath eastern China. J. Petrol. 47, 2233–2256.
Zheng, J.P., Griffin, W.L., O'Reilly, S.Y., Yu, C.M., Pearson, N., Zhang, M., 2007. Mechanism and timing of lithospheric modification and replacement beneath the eastern North China Craton: peridotitic xenoliths from the 100 Ma Fuxin basalts and a regional synthesis. Geochim. Cosmochim. Acta 71, 5203–5225.
Zheng, J.P., O'Reilly, S.Y., Griffin, W.L., Lu, F.X., Zhang, M., Pearson, N.J., 2001. Relict refracoty mantle beneath the eastern North China block: Significance for lithosphere evolution. Lithos 57, 43–66.
Zheng, Y.F., Fu, B., Gong, B., 2003. Stab le isotope geochemistry of ultraist pressure metamorphic rocks from the Dabie-Sulu orogen in China: implications for geodynamics and fluid regime. Earth Sci. Rev. 62, 105–161.
Zhou, X.W., Zhao, G.C., Wei, C.J., Geng, Y.S., Sun, M., 2008. Metamorphic evolution and

Th-U-Pb zircon and monazite geochronology of high-pressure pelitic granulites in the Jiaobei massif of the North China Craton. American J. Sci. 308, 328–350.
Zhu, G., Hu, Z.Q., Chen, Y., Niu, M.L., Xie, C.L., 2008. Evolution of early Cretaceous extensional basins in the eastern North China Craton and its implicaiton for the craton destruction. Geol. Bull. China 27, 1594–1604 (in Chiense with English abstract).
Zou, H.B., Zindler, A., Xu, X.S., Qi, Q., 2000. Major, trace element, and Nd, Sr and Pb isotope studies of Cenozoic basalts in SE China Mantle sources, regional variations and tectonic significance. Geol. 171, 33–47.